Published March 2, 2017

Inhibition of the mitochondrial pyruvate carrier protects from excitotoxic neuronal death

Ajit S. Divakaruni,[1] Martina Wallace,[2] Caodu Buren,[5] Kelly Martyniuk,[3] Alexander Y. Andreyev,[1] Edward Li,[5] Jerel A. Fields,[4] Thekla Cordes,[2] Ian J. Reynolds,[6] Brenda L. Bloodgood,[3] Lynn A. Raymond,[3] Christian M. Metallo,[2] and Anne N. Murphy[1]

[1]Department of Pharmacology, [2]Department of Bioengineering, [3]Division of Biological Sciences, Neurobiology Section, and [4]Department of Pathology, University of California, San Diego, La Jolla, CA 92093
[5]Department of Psychiatry, University of British Columbia, Vancouver, British Columbia V6T 1Z3, Canada
[6]Discovery Research, Teva Pharmaceutical Industries Ltd., West Chester, PA 19380

Glutamate is the dominant excitatory neurotransmitter in the brain, but under conditions of metabolic stress it can accumulate to excitotoxic levels. Although pharmacologic modulation of excitatory amino acid receptors is well studied, minimal consideration has been given to targeting mitochondrial glutamate metabolism to control neurotransmitter levels. Here we demonstrate that chemical inhibition of the mitochondrial pyruvate carrier (MPC) protects primary cortical neurons from excitotoxic death. Reductions in mitochondrial pyruvate uptake do not compromise cellular energy metabolism, suggesting neuronal metabolic flexibility. Rather, MPC inhibition rewires mitochondrial substrate metabolism to preferentially increase reliance on glutamate to fuel energetics and anaplerosis. Mobilizing the neuronal glutamate pool for oxidation decreases the quantity of glutamate released upon depolarization and, in turn, limits the positive-feedback cascade of excitotoxic neuronal injury. The finding links mitochondrial pyruvate metabolism to glutamatergic neurotransmission and establishes the MPC as a therapeutic target to treat neurodegenerative diseases characterized by excitotoxicity.

Introduction

Healthy cell function in peripheral tissues is characterized by the ability of metabolism to adapt to changes in nutrient availability and oxidize multiple energy substrates (Muoio, 2014; Stanley et al., 2014; Olson et al., 2016). For example, skeletal muscle will readily switch from robust use of fatty acids during fasting to substantial glucose oxidation upon feeding. This metabolic flexibility is a characteristic of healthy skeletal muscle, and an impaired ability to shift between oxidation of fatty acids and glucose in response to nutrient availability and hormonal status is associated with obesity, insulin resistance, and reduced aerobic fitness (Kelley, 2005; Muoio, 2014). A loss of metabolic plasticity is associated with disease pathogenesis in not only type 2 diabetes, but also cardiac disease (Fillmore and Lopaschuk, 2013) and even certain cancers, where the metabolic changes associated with tumorigenesis can include a hardwired reliance on specific metabolic pathways (Tennant et al., 2010; Pavlova and Thompson, 2016).

Unlike peripheral tissues, however, it is generally accepted that the brain lacks considerable metabolic flexibility. Glucose is its obligatory substrate (Clarke and Sokoloff, 1994; Bélanger et al., 2011; McKenna et al., 2012), and the brain is thought to rarely oxidize nonglucose substrates apart from ketone bodies during starvation (Cunnane et al., 2011). Despite a substantial energy demand, the brain has a limited capacity to store glycogen or use gluconeogenesis to compensate for changes in glucose provision, so changes in blood glucose supply can have profound effects on brain function if the arterial concentration drops appreciably (Clarke and Sokoloff, 1994; Cryer, 2007).

Multiple forms of neurodegenerative disease are associated with energetic and metabolic deficits (Johri and Beal, 2012), and links between insufficient metabolic plasticity and neurodegeneration are emerging as well. For example, hypometabolism of glucose can manifest long before clinical symptoms in Alzheimer's disease (Cunnane et al., 2011), and epidemiological data consistently link insulin resistance with an increased risk of cognitive impairment (Cunnane et al., 2011; Craft, 2012; de la Monte, 2012). Links between metabolic inflexibility and disease etiology are further underscored by evidence that oxida-

Correspondence to Anne N. Murphy: anmurphy@ucsd.edu

A.S. Divakaruni's present address is Dept. of Molecular and Medical Pharmacology, University of California, Los Angeles, Los Angeles, CA 90095.

Abbreviations used: BCAA, branched chain amino acid; DIV, days in vitro; FCCP, carbonyl cyanide-4-(trifluoromethoxy)phenylhydrazone; GABA, γ-aminobutyric acid; LDH, lactate dehydrogenase; MPC, mitochondrial pyruvate carrier; MPE, molar percent enrichment; NMDA, *N*-methyl-D-aspartate; PDH, pyruvate dehydrogenase; PFO, perfringolysin O; vGlut1, vesicular glutamate transporter 1.

Supplemental Material can be found at:
/content/suppl/2017/03/01/jcb.201612067.DC1.html

The Rockefeller University Press $30.00
J. Cell Biol. Vol. 216 No. 4 1091–1105
https://doi.org/10.1083/jcb.201612067

Published March 2, 2017

tion of nonglucose substrates may be beneficial in certain forms of neurodegeneration. For example, mouse models that reduce the capacity of neurons and astrocytes to oxidize glucose but promote ketone body oxidation exhibit resistance to epileptic seizures (Giménez-Cassina et al., 2012). This aligns with the longstanding observation that low-carbohydrate diets can confer dramatic benefits to some forms of medically refractory seizure disorders (Hartman et al., 2007). In fact, this promise has triggered the clinical evaluation of ketogenic diets for several forms of acute and chronic neurodegenerative disease, although a mechanistic understanding of the potential benefits remains unresolved (Masino and Rho, 2012; Lutas and Yellen, 2013).

An overlap between oxidation of specific metabolic substrates and neuronal physiology could exist at handling of amino acids, which are indispensable for neurotransmission but can also be used as metabolic substrates (Yudkoff et al., 2008; McKenna et al., 2012). In the mammalian central nervous system, glutamate is the dominant excitatory neurotransmitter (balanced with inhibitory γ-aminobutyric acid [GABA]) and is responsible for the synaptic plasticity associated with learning and memory (Meldrum, 2000). During glutamatergic neurotransmission, packaged glutamate in a presynaptic neuron is released to the synapse, where it binds to ionotropic and metabotropic receptors on postsynaptic neurons to trigger activity. It is then rapidly cleared by high-affinity transporters, allowing a continuous cycle of neurotransmitter activity (Maragakis and Rothstein, 2001). Maintaining homeostatic levels of synaptic glutamate comes at a tremendous energetic cost (Nicholls, 2009), and predictably, periods of metabolic stress result in dysregulated glutamate handling (Choi and Rothman, 1990). When glutamate rises to toxic levels, excessive receptor stimulation triggers intracellular Ca^{2+} overload that subsequently causes mitochondrial complex I dysfunction (Kushnareva et al., 2005) and activates neurotoxic signaling cascades (Szydlowska and Tymianski, 2010). Glutamate excitotoxicity not only is a hallmark of acute neuropathologies, such as epilepsy, stroke, and traumatic brain injury, but is also thought to contribute to progressive neurodegenerative diseases including Alzheimer's disease (Coyle and Puttfarcken, 1993).

In many peripheral tissues, metabolism of glutamate (and glutamine) is essential for energetics, biosynthesis, redox homeostasis, and hormonal control of metabolism (DeBerardinis and Cheng, 2010). However, this stands in stark contrast to the conventional central nervous system model, in which glutamate metabolism is widely considered to be compartmentalized within the glutamine-glutamate cycle because of its central role in neurotransmission (Daikhin and Yudkoff, 2000; McKenna et al., 2012; Schousboe et al., 2013). In the canonical model, astrocytes supply glutamine to neurons, where it is deamidated to glutamate, packaged into vesicles, released to the extracellular space to activate glutamate receptors, and sequestered by astrocytes for resynthesis of glutamine. It is sometimes acknowledged that glutamate metabolism is closely associated with TCA cycle function, although the focus is often on astrocytic metabolism (Daikhin and Yudkoff, 2000; Yudkoff et al., 2008; McKenna et al., 2012; Schousboe et al., 2013). As such, the concept of whether alterations in TCA cycle metabolism can adjust neuronal glutamate handling, vesicular release, and excitotoxic injury remains largely unconsidered.

To reconcile the potential benefits from oxidation of nonglucose substrates with the perceived, inexorable dependence of neuronal metabolism on glucose, we mapped the pattern of cellular metabolism in response to reduced mitochondrial pyruvate carrier (MPC) activity. The MPC is an inner-membrane transporter that facilitates pyruvate uptake from the cytoplasm into mitochondria (Bricker et al., 2012; Herzig et al., 2012). It is a central regulator of mitochondrial substrate utilization (Vacanti et al., 2014), and restrictions in mitochondrial pyruvate uptake can potentiate the use of fatty acids and a range of amino acids to fuel cellular energetics and biosynthesis (Vacanti et al., 2014; Yang et al., 2014; Gray et al., 2015; McCommis et al., 2015).

Broadly, mapping the pattern of neuronal metabolism upon MPC inhibition allowed us to (a) determine the extent of metabolic flexibility in neurons and (b) determine whether adjustments in neuronal substrate oxidation could affect susceptibility to injury. We report that neuronal metabolism is characterized by metabolic plasticity, and oxidative metabolism can be maintained in spite of large reductions in mitochondrial pyruvate uptake because of a selective increase in glutamate oxidation. As such, and perhaps counterintuitively, reductions in mitochondrial pyruvate metabolism can be neuroprotective: increased glutamate oxidation decreases the glutamate available for synaptic release and, in turn, minimizes the positive feedback cascade of excitotoxic injury.

Results

Cortical neurons remain viable in culture after inhibition of MPC activity

Before exploring neuronal metabolic flexibility, it was first necessary to determine whether primary cortical neurons remain viable in response to restricted mitochondrial pyruvate uptake. This was assessed by treatment with the specific MPC inhibitor UK5099 (Hildyard et al., 2005; Fig. 1, a and b). Surprisingly, neurons maintained in standard culture conditions remained viable over 72 h of treatment (Fig. 1 c). UK5099 reduced the maximal capacity of neurons to oxidize pyruvate by >50% (Fig. 1 d) but, unlike the respiratory complex III inhibitor antimycin A, did not cause cell death. This difference demonstrates that blocking mitochondrial pyruvate uptake elicits a different metabolic response than respiratory chain inhibition. Moreover, it suggests that neurons have a significant, inherent capacity to oxidize nonglucose substrates (stored endogenously or provided in culture medium) to meet their energetic and metabolic demands.

Neurons readily oxidize nonglucose substrates

Having demonstrated that viability was unchanged upon reduced mitochondrial pyruvate uptake, we then characterized the capacity of neurons to drive cellular energetics with alternative substrates. Initially, we chose to focus on ketone bodies, as the brain is known to oxidize these during starvation, and branched chain amino acids (BCAAs), as significant BCAA oxidation is observed in some terminally differentiated cells (Vacanti et al., 2014; Green et al., 2016). Respirometry in permeabilized cells demonstrated that neuronal mitochondria can oxidize not only canonical mitochondrial substrates (pyruvate/malate, succinate/rotenone, glutamate/malate) and ketone bodies (β-hydroxybutyrate), but also the branched chain keto-acid catabolites of leucine, isoleucine, and valine (Figs. 2 a and S1 a).

To measure alternative substrate oxidation in the context of intact neurons, we conducted bioenergetic experiments in customized medium modeled after culture conditions but

Published March 2, 2017

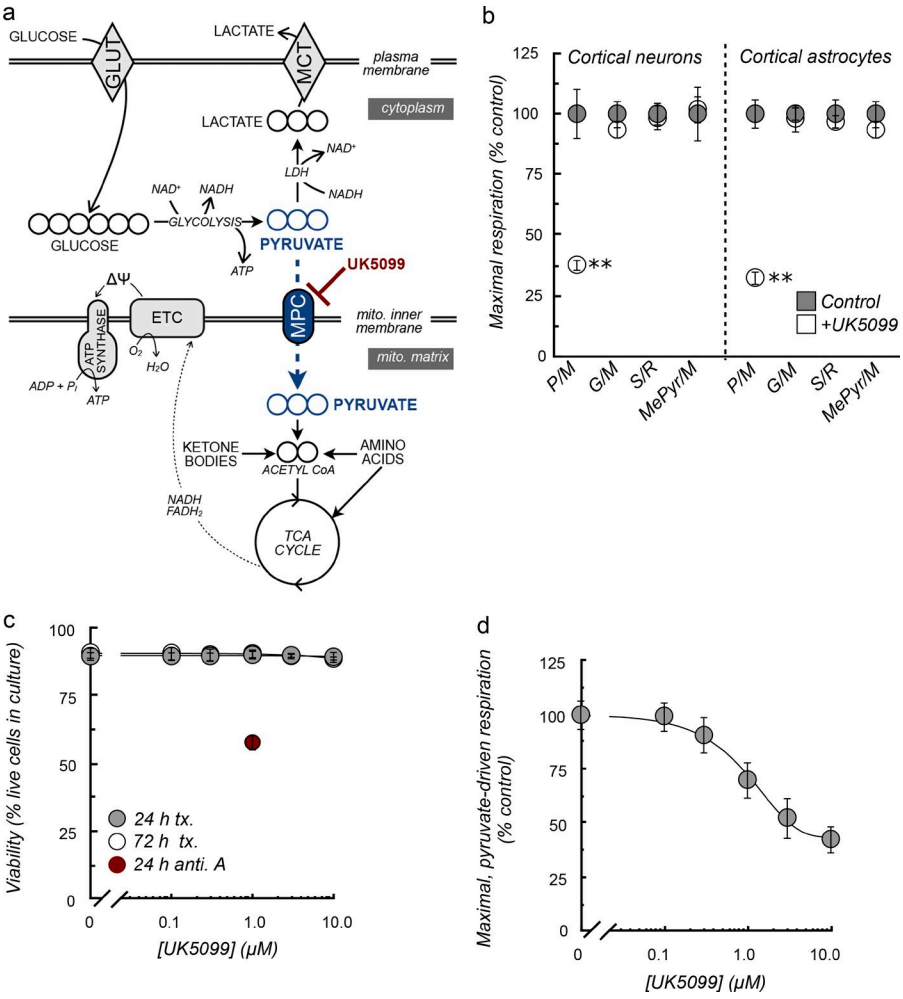

Figure 1. **Neuronal viability is maintained despite MPC inhibition.** (a) The MPC (blue) sits at a central hub of cellular energetics, facilitating transport of cytoplasmic pyruvate into the mitochondrial (mito.) matrix. GLUT, glucose transporter; MCT, monocarboxylate transporter; ETC, electron transport chain. (b–d) All data are $n = 4$; presented as mean ± SEM. **, $P < 0.01$. (b) Uncoupler-stimulated respiration in permeabilized cortical neurons and astrocytes in response to 5 μM UK5099 demonstrates specific inhibition of facilitated pyruvate transport. Treatment was made acutely in assay medium lacking albumin. P/M, 5 mM pyruvate with 1 mM malate and 2 mM dichloroacetate; G/M, 5 mM glutamate with 5 mM malate; S/R, 10 mM succinate with 2 μM rotenone; and MePyr/M, 25 mM methyl pyruvate with 5 mM pyruvate, 1 mM malate, and 2 mM dichloroacetate. (c) Viability of rat cortical neuronal cultures in response to UK5099 or 1 μM antimycin A (anti. A) treatment (tx.). (d) Efficacy of UK5099 is demonstrated in neurons by measuring FCCP-stimulated, pyruvate-driven respiration in permeabilized cells after 24-h drug treatment.

lacking respiratory substrates, allowing substrate provision to be experimentally controlled (Table 1). We estimated the ATP production rate from oxidative phosphorylation and glycolysis by applying known stoichiometries to rates of respiration and lactate efflux and used UK5099 to acutely restrict mitochondrial pyruvate uptake and potentiate use of other substrates. Predictably, neurons offered only glucose and pyruvate in this medium increased their glycolytic rate but could not meet their overall ATP demand in response to 90-min UK5099 treatment. The altered rates of glycolysis and total ATP production, however, were entirely reversed when this simplified medium was supplemented with β-hydroxybutyrate and leucine (Fig. 2 b). In fact, carbonyl cyanide-4-(trifluoromethoxy)phenylhydrazone (FCCP)–stimulated respiration indicated that cortical neurons have a remarkable capacity to fuel respiration using these alternative energy substrates that far exceeds what is required to meet the basal cellular energy requirements (Fig. 2 c and Fig. S1, b and c). These experiments reveal that neurons have a substantial capacity to oxidize nonglucose substrates, but provide little information about whether, and to what extent, these substrates are used in rich cell culture medium.

We therefore used stable isotope tracers ([$^{13}C_6$]glucose, [$^{13}C_4$]β-hydroxybutyrate, or [$^{13}C_6$]leucine) and mass spectrometry to further characterize neuronal oxidation of alternative substrates under basal conditions. These experiments were conducted in rich medium replete with a broad complement of amino acids and oxidizable substrates (Neuro-c; see Materials and methods and Table 1). Incorporation of isotopically labeled carbon into TCA intermediates can provide quantitative information about the relative flux of each substrate into the TCA cycle (Fig. S1 d). Additionally, as acetyl CoA serves as the precursor for de novo lipogenesis, labeling of total palmitate can be reliably used to quantify isotope incorporation into the lipogenic acetyl CoA pool with isotopomer spectral analysis (Fig. S1 e).

We found that nonglucose substrates contributed significantly to the lipogenic acetyl CoA pool (Fig. 2 d) and enriched TCA cycle intermediates (Fig. 2, e and f; and Fig. S1, f and g). Leucine-derived carbon enriched TCA cycle intermediates and, surprisingly, accounted for nearly half as much lipogenic acetyl CoA as glucose (Fig. 2 d). The relative incorporation of leucine into fatty acids and citrate was comparable to that of differentiated adipocytes (Green et al., 2016) and human skeletal muscle myotubes (Vacanti et al., 2014), suggesting that leucine may be a more significant oxidative and biosynthetic carbon source in neurons than is generally appreciated (Kajimoto et al., 2014). Further demonstration of neuronal metabolic plasticity was apparent when culture medium was supplemented with 2 mM β-hydroxybutyrate. Mitochondrial glucose utilization significantly decreased as previously observed (Lund et al., 2009), and the contribution of β-hydroxybutyrate to de novo lipogenesis and enrichment of TCA cycle intermediates was greater than or equal to those of glucose (Fig. 2, e and f; and Fig. S1, f and g). The combination of respirometry and stable isotope tracing reveals that neurons have an intrinsic capacity to drive energetics

Published March 2, 2017

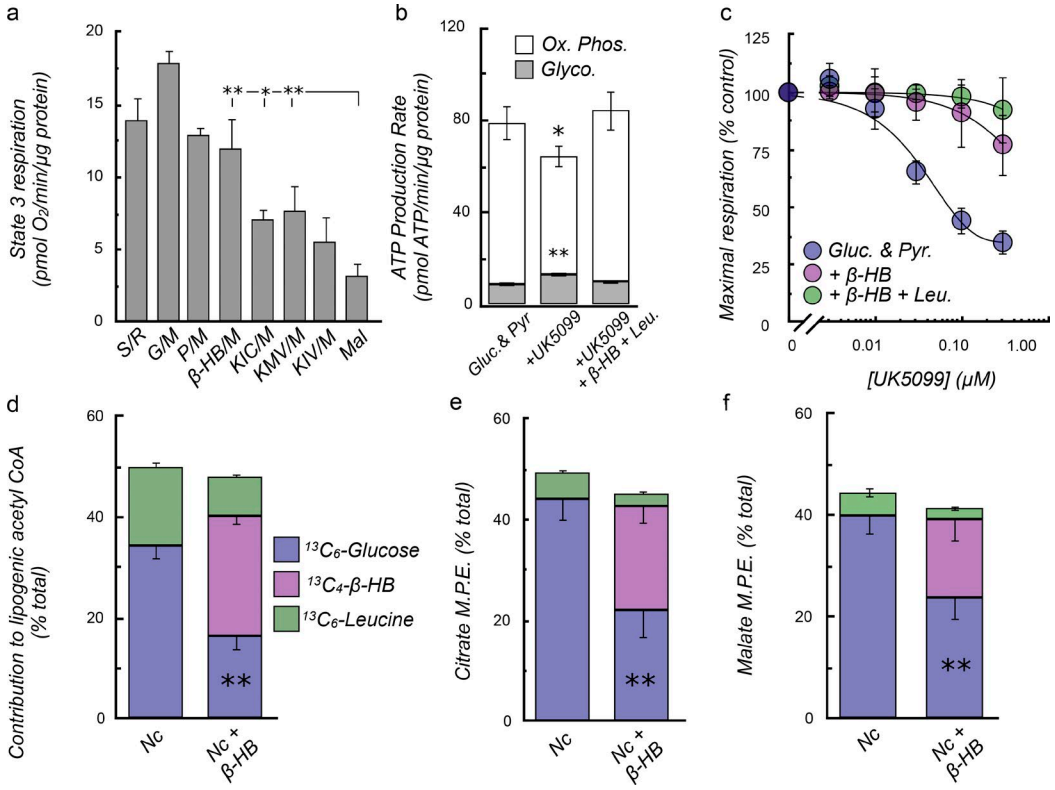

Figure 2. **Metabolic flexibility in primary cortical neurons.** (a) ADP-stimulated respiration in permeabilized neurons shows that neuronal mitochondria can oxidize a variety of substrates (n = 3). S/R, 10 mM succinate with 2 µM rotenone; G/M, 5 mM glutamate with 5 mM malate; P/M, 5 mM pyruvate with 1 mM malate and 2 mM dichloroacetate; β-HB/M, 5 mM β-hydroxybutyrate with 1 mM malate; KIC/M, 5 mM α-ketoisocaproate with 1 mM malate; KMV/M, 5 mM α-keto-β-methylvalerate with 1 mM malate; KIV/M, 5 mM α-ketoisovalerate with 1 mM malate; and M, 1 mM malate. (b) UK5099 does not compromise rates of ATP production in intact neurons when β-hydroxybutyrate and leucine are added to medium containing glucose and pyruvate. Total ATP production rates are estimated as the sum of ATP produced from oxidative phosphorylation (Ox. Phos.) and glycolysis (Glyco.); [glucose], 10 mM; [pyruvate], 1 mM; [β-hydroxybutyrate], 3 mM; [leucine], 2 mM; [UK5099], 0.1 µM for 90 min. (c) Maximal, FCCP-stimulated respiration is maintained despite MPC inhibition when medium is supplemented with β-hydroxybutyrate and leucine (concentrations as in b). n = 5. (d–f) The extent to which glucose, β-hydroxybutyrate, and leucine are metabolized under control, unchallenged conditions was determined with stable isotope tracing in rich culture medium over 24 h. Nc, Neuro-c rich medium; Nc + β-HB, Neuro-c with 2 mM β-hydroxybutyrate. [leucine], 0.8 mM. (d) β-Hydroxybutyrate and leucine contribute significantly to the lipogenic acetyl CoA as determined by isotopomer spectral analysis (ISA). (e and f) MPE of labeled carbon into citrate (e) and malate (f) also shows incorporation of β-hydroxybutyrate and leucine into TCA cycle pools. Conditions as in d. Unless stated otherwise, all data are n = 4 and presented as mean ± SEM. *, P < 0.05; **, P < 0.01.

and biosynthesis with alternative mitochondrial substrates, and do so at substantial rates under basal conditions.

Bioenergetics are maintained upon MPC inhibition despite a negligible increase in β-hydroxybutyrate and leucine oxidation

Establishing that neurons are metabolically flexible allowed us to subsequently characterize the metabolic adaptations to reductions in mitochondrial pyruvate uptake, with the ultimate goal of studying whether enforcing oxidation of nonglucose substrates could be beneficial to neurons. After treating neurons in rich culture medium with UK5099 for 24 h to increase their reliance on alternative mitochondrial substrates, we quantified isotope enrichment into TCA cycle intermediates. Upon treatment, incorporation of glucose-derived carbon into the TCA cycle was significantly reduced (Figs. 3 a and S2 a), as expected. A profound reduction in mitochondrial pyruvate uptake, however, did not compromise global mitochondrial bioenergetics. Basal respiration rates were entirely maintained (Fig. 3 b) without a significant change in intracellular lactate levels (Fig. 3 c), indicating no substantial change in the balance between oxidative phosphorylation and glycolysis. Additionally, rates of de novo palmitate synthesis were not significantly changed upon chemical MPC inhibition (Fig. S2 b). Collectively, these results suggest that mitochondrial oxidation of nonglucose substrates was increased to maintain the metabolic requirements of the cell.

Given the substantial capacity of neurons to oxidize β-hydroxybutyrate and leucine (Fig. 2), we first hypothesized that oxidation of these substrates was increased to compensate for decreased mitochondrial pyruvate uptake. Unexpectedly, however, there was little to no increase in the oxidation of these substrates upon UK5099 treatment. Incorporation of carbon derived from β-hydroxybutyrate or leucine into TCA cycle intermediates was largely unchanged (Fig. 3, d and e), and their contribution to the lipogenic acetyl CoA pool was only marginally increased despite a two-thirds reduction in lipogenesis from glucose-derived carbon (Fig. 3 f). These data indicate that neurons adapt to MPC inhibition in rich medium by increasing oxidation of a previously unconsidered substrate.

Glutamate oxidation is specifically increased upon MPC inhibition to maintain anaplerosis

To better understand the metabolic adaptation of neurons to MPC inhibition, we measured abundances of TCA cycle intermediates and amino acids. We observed significant changes

Published March 2, 2017

Table 1. **Neuro-c medium composition**

Item	Concentration
	mM
Amino acids	
Glycine	0.40
L-Alanine	0.02
L-Arginine	0.40
L-Asparagine	0.01
L-Cysteine	0.26
L-Histidine	0.20
L-Isoleucine	0.80[a]
L-Leucine	0.8–2.0[a]
L-Lysine	0.80
L-Methionine	0.20
L-Phenylalanine	0.40
L-Proline	0.07
L-Serine	0.40
L-Threonine	0.80
L-Tryptophan	0.08
L-Tyrosine	0.40
L-Valine	0.80[a]
Vitamins	
Choline chloride	0.029
D-Calcium pantothenate	0.008
Folic acid	0.009
Niacinamide	0.033
Pyridoxal hydrochloride	0.02
Riboflavin	0.001
Thiamine hydrochloride	0.012
Vitamin B12	5.02×10^{-6}
i-Inositol	0.04
Inorganic salts	
Calcium chloride	1.801
Ferric nitrate	2.48×10^{-4}
Magnesium chloride	0.814
Potassium chloride	5.333
Sodium chloride	51.724
Sodium phosphate (monobasic)	0.906
Zinc sulfate	6.74×10^{-4}
Additives	
Sodium bicarbonate	26.19 mM[a]
Hepes	5-10.9 mM[a]
Phenol red	0.02 mM
B27 supplements	2% (vol/vol)[a]
GlutaMAX	2 mM[a]
Penicillin	100 U/ml[a]
Streptomycin	100 µg/ml[a]
L-Glutamine	0.5–2.0 mM[a]
Glucose	8–10 mM[a]
Pyruvate	0.22–1.0 mM[a]
β-Hydroxybutyrate	2–3 mM[a]

[a]Added as indicated further in the text.

in the intracellular abundance of glutamate and aspartate, as UK5099 treatment dropped total glutamate levels by ∼50%, with a concomitant, twofold increase in aspartate (Figs. 4 a and S2 c). Notably, overall abundances of other amino acids and TCA cycle intermediates were not significantly changed (Fig. S2 d), apart from decreases in citrate and alanine (because of reduced mitochondrial pyruvate uptake [Vacanti et al., 2014]) as well as proline (a direct metabolite of glutamate). This pattern of metabolic reprogramming is consistent with that observed upon MPC inhibition in immortalized and primary cells including myocytes, cancer cells, and the retina, and suggests increased oxidation of glutamate via aspartate aminotransferase (Bricker et al., 2012; Du et al., 2013; Vacanti et al., 2014; Yang et al., 2014; Gray et al., 2015).

In the context of other cell types, the result would perhaps be unsurprising: glutamine is appreciated as an important energetic and biosynthetic substrate, particularly in cancerous or highly proliferative cells (DeBerardinis and Cheng, 2010). In neuronal physiology, however, it is widely perceived that glutamate metabolism in the brain is compartmentalized as a neurotransmitter (Daikhin and Yudkoff, 2000; McKenna et al., 2012; Schousboe et al., 2013). The data in Fig. 4 a, however, suggest that the abundance of the neuronal glutamate pool can be readily adjusted by TCA cycle metabolism. Moreover, isotope enrichment of glutamate and aspartate mirrored the composition of TCA cycle intermediates during studies of neuronal metabolic plasticity described earlier (Fig. S2, e and f, relative to Fig. 2, e and f; and Fig. S1, f and g). This suggests that glutamate is synthesized de novo from glucose and other TCA cycle substrates and is consistent with recent in vivo metabolic tracing from human and rodent brains (Marin-Valencia et al., 2012; Tardito et al., 2015). Collectively, the data demonstrate that both the abundance and the molecular composition of the neuronal glutamate pool can be adjusted by TCA cycle metabolism.

We subsequently tested the hypothesis that glutamate oxidation is specifically up-regulated in response to reduced pyruvate oxidation. Neurons cannot be offered exogenous glutamate as a respiratory substrate, most notably because it will cause excitotoxic cell death from excessive *N*-methyl-D-aspartate (NMDA) receptor agonism. However, in addition to its synthesis from α-ketoglutarate via transamination, glutamate is derived at significant rates from glutamine via deamidation. We therefore conducted a series of experiments in which stabilized L-alanyl-L-glutamine (GlutaMAX) in neuronal culture medium was replaced with [$^{13}C_5$]glutamine to track incorporation of glutamine-derived carbon (Fig. S3 a). The NMDA receptor antagonist MK801 was included to prevent excitotoxic injury from glutamate generated by spontaneous deamidation of glutamine. Over 24 h, UK5099 treatment profoundly increased glutamine uptake (Fig. 4 b), flux of glutamine-derived acetyl CoA to newly synthesized palmitate (Fig. 4 c), and enrichment from glutamine-derived carbon into TCA cycle intermediates (Figs. 4 d and S3 b). Consistent with this observation, cortical neurons can also use glutamine to fuel respiration in response to MPC inhibition (Fig. S3 c).

Metabolic alterations in the cytoplasm were further indicative of enhanced glutamate oxidation. Global respiratory inhibition and a shift from oxidative phosphorylation to glycolysis generally results in an oxidized cytoplasm (increased NAD^+/NADH ratio) caused by a decreased pyruvate/lactate ratio. Upon neuronal MPC inhibition, however, the pyruvate/lactate ratio increased (Fig. 3 c), and glucose-derived carbon was incorporated to a greater extent into pyruvate and serine relative to lactate (Fig. 4 e). This suggests a more reduced cytoplasm (Fig. S3 d), perhaps helping to drive glutamate oxidation by making the malate-aspartate shuttle more energetically favorable (Fig. S3 e).

Naturally, a question arises as to why glutamate oxidation is preferentially increased in neurons upon MPC inhibition, rather than a broad increase in the oxidation of multiple other substrates observed in other systems (Vacanti et al., 2014; Gray et al., 2015). We speculated that this might be to compensate

Published March 2, 2017

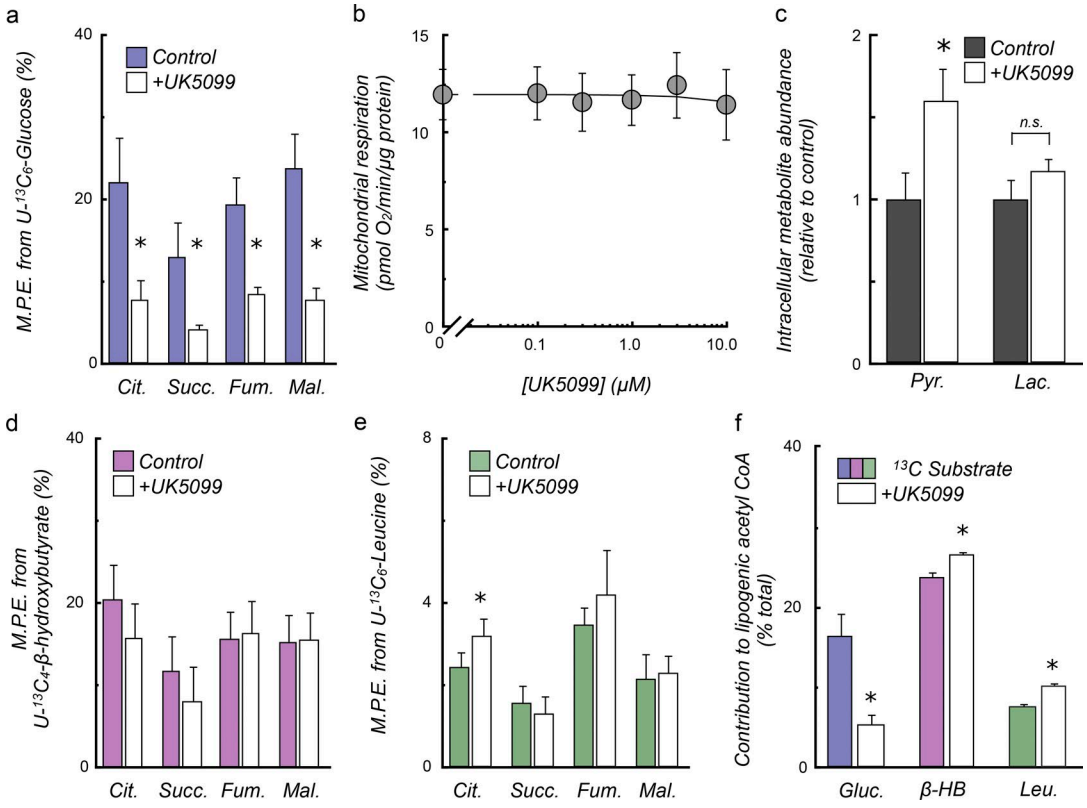

Figure 3. **Neuronal MPC inhibition does not compromise bioenergetics despite little/no increase in ketone body or leucine oxidation.** (a) MPE of [U-$^{13}C_6$] glucose indicates that UK5099 treatment restricts incorporation of glucose carbon into TCA cycle intermediates. (b) Basal mitochondrial respiration is not compromised after 24-h UK5099 treatment. n = 3. (c) MPC inhibition increases the intracellular abundance of pyruvate without a significant change in lactate. (d and e) Treatment with UK5099 does not cause generalized increases in MPE from [U-$^{13}C_4$]β-hydroxybutyrate (d) or leucine (e) into TCA cycle intermediates. (f) Relative contribution from [U-$^{13}C_6$]glucose to lipogenic acetyl CoA is substantially decreased upon reduced pyruvate uptake, with slight increases from [U-$^{13}C_4$]β-hydroxybutyrate and [U-$^{13}C_6$]leucine. All experiments were conducted in Neuro-c as in Fig. 2 (d–f) and detailed in Materials and methods. Data are n = 4 unless otherwise noted and presented as mean ± SEM. In a and c–f: [UK5099], 10 µM for 24 h. β-HB, β-hydroxybutyrate; Cit., citrate; Fum., fumarate; Gluc., glucose; Lac., lactate; Leuc., leucine; Mal., malate; Pyr., pyruvate; Succ., succinate. *, P < 0.05; n.s., not significant.

for reductions in glucose anaplerosis (Chinopoulos, 2013). In addition to generating acetyl CoA via pyruvate dehydrogenase (PDH), pyruvate can be converted to the TCA cycle intermediates oxaloacetate or malate via the CO_2-fixing reactions of pyruvate carboxylase or malic enzyme (Fig. 4 f; Hassel, 2001; Chinopoulos, 2013). These anaplerotic reactions add net carbon to the TCA cycle, replenishing pools of intermediates that are siphoned off for biosynthesis. Conversely, PDH, or any reaction that provides carbon to the TCA cycle via acetyl CoA, does not contribute net carbon to the TCA cycle (Figs. 4 f and S1 d). If UK5099 restricted a major source of anaplerosis, the compensatory response could not simply be to increase oxidation of substrates that generate acetyl CoA (such as β-hydroxybutyrate and leucine), but would instead require a substrate that also adds net carbon to the TCA cycle (i.e., glutamate).

Significant differences in the citrate mass isotopomer distributions from glucose and β-hydroxybutyrate provided initial hints of significant neuronal glucose anaplerosis under basal conditions (Fig. S3 f). To definitively test this, we offered neurons a [3-$^{13}C_1$]glucose tracer, which contains an isotopic label on the third glucose carbon. This label is lost when pyruvate is oxidized via PDH but is retained on TCA cycle intermediates if pyruvate is metabolized via anaplerotic reactions (Fig. 4 f). We observed substantial labeling from this tracer in citrate, malate, and aspartate (via oxaloacetate transamination). Labeling was significantly decreased by UK5099 (Fig. 4 g) and directly attributable to anaplerotic reactions rather than PDH (Fig. S3 g). As such, decreased glucose anaplerosis upon MPC inhibition provides a rationale for a preferential increase in glutamate oxidation.

Organotypic hippocampal cultures show reciprocal oxidation of pyruvate and glutamate

Next, we tested whether the metabolic profile observed upon MPC inhibition in pure neuronal cultures could extend to a more complex and representative model of brain tissue function. For this, we used organotypic hippocampal slice cultures, which retain many aspects of the cellular heterogeneity and synaptic architecture of the tissue (Gähwiler et al., 1997). Although neuron-specific oxidation of glutamate cannot be discerned given the multicellular nature of slice cultures, this system can nonetheless be used to broadly test whether the metabolic profile of MPC inhibition persists in a more intact model system. We treated hippocampal slice cultures with 10 µM UK5099 for 48 h in the presence of isotopic tracers. This elicited a small but significant decrease in citrate enrichment from uniformly labeled glucose (Fig. 5 a), indicating a modest reduction in mitochondrial pyruvate uptake. Indeed, the resulting metabolic profile in slice cultures reproduced the hallmarks seen in dissociated neuronal cultures: (a) enrichment from glucose-derived carbon preferentially into pyruvate and serine rather than lac-

Published March 2, 2017

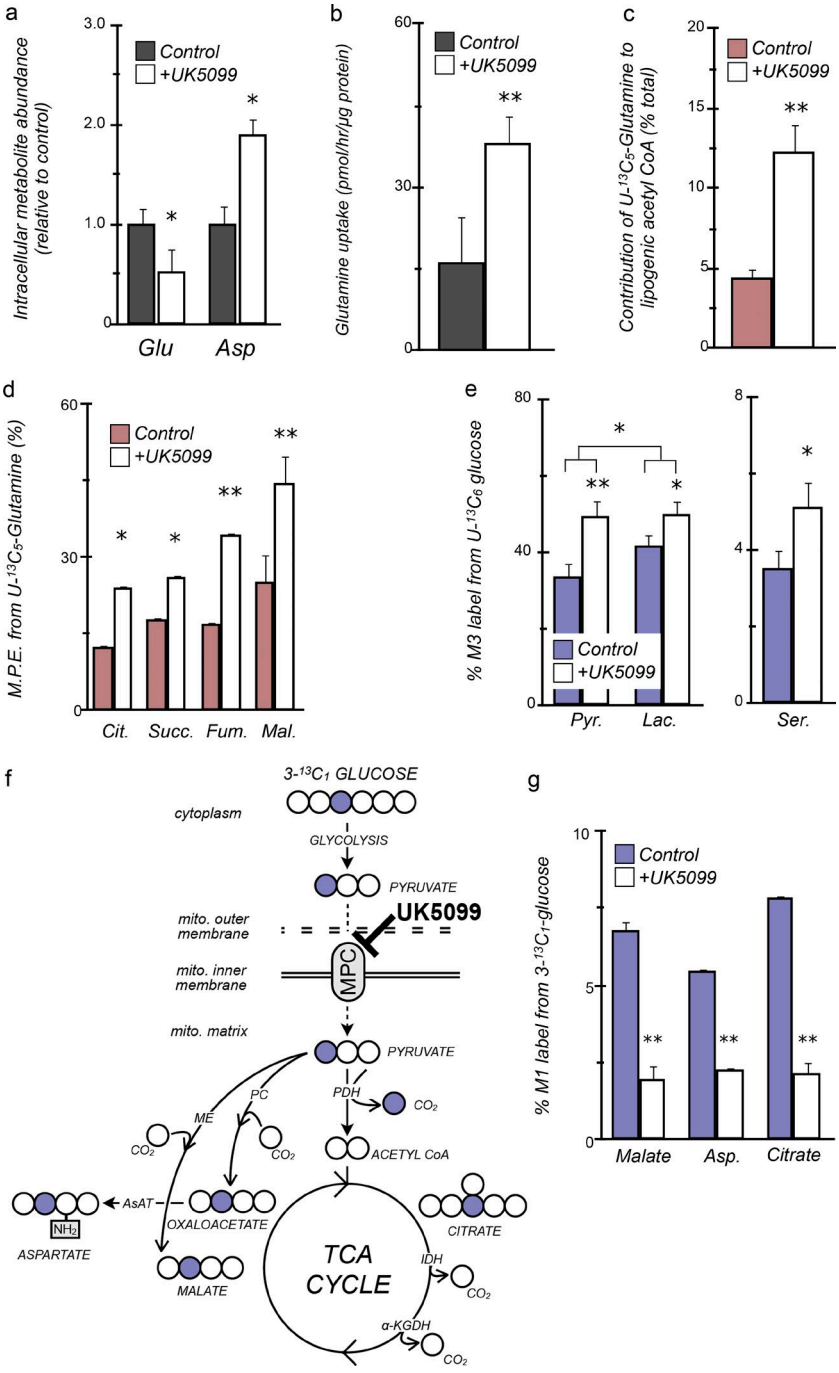

Figure 4. **Glutamate oxidation is selectively up-regulated upon MPC inhibition to maintain anaplerosis in cortical neurons.** (a) Relative intracellular abundance of glutamate (Glu) decreases and aspartate (Asp) increases. (b) Uptake of glutamine, a precursor of glutamate, increases from the extracellular medium. (c) Relative contribution of [U-$^{13}C_5$]glutamine to the lipogenic acetyl CoA pool is enhanced. (d) MPE of [U-$^{13}C_5$]glutamine incorporated into TCA cycle intermediates increases. (e) Enrichment from [U-$^{13}C_6$]glucose demonstrates greater proportional increases in fully labeled pyruvate and serine compared with lactate. (f) Schematic depicting use of a [3-$^{13}C_1$]glucose tracer to demonstrate glucose anaplerosis. The labeled carbon is lost via the PDH reaction but retained by the anaplerotic reactions of pyruvate carboxylase (PC) and malic enzyme (ME). The two-carbon intermediate acetyl CoA does not add net carbon to the TCA cycle because CO_2 is lost in both the isocitrate dehydrogenase (IDH) and α-ketoglutarate dehydrogenase (α-KGDH) reactions. (g) UK5099 treatment lowers the percentage of single-labeled carbon from [3-$^{13}C_1$] glucose on malate, citrate, and aspartate, indicating significant flux from glucose through anaplerotic reactions. All experiments were conducted in Neuro-c medium as detailed in Materials and methods, with comparisons made between control conditions and 10 μM UK5099 treatment for 24 h. Data are $n = 4$ unless otherwise stated and are presented as mean ± SEM. Asp, aspartate; Glu, glutamate; Pyr., pyruvate; Ser., serine. *, $P < 0.05$; **, $P < 0.01$.

tate (Fig. 5 b), (b) increased ratios of aspartate/glutamate and pyruvate/lactate (Fig. 5 c), and (c) a slight but significant increase in enrichment from glutamine-derived carbon into citrate (Fig. 5 d). This reciprocal regulation of pyruvate and glutamate oxidation is consistent with earlier results and supports the concept that pyruvate metabolism by the TCA cycle can regulate glutamate handling in intact, multicellular neural systems.

MPC inhibition protects from excitotoxic cell death by lowering evoked glutamate release

Under conditions of metabolic stress that excessively depolarize neurons, synaptic glutamate rises to excitotoxic levels that exacerbate neuronal injury. Therefore, having shown that blocking mitochondrial pyruvate uptake lowers the intraneuronal glutamate pool, we tested whether it also reduces the glutamate pool released upon plasma membrane depolarization. Indeed, neurons treated with UK5099 released less glutamate to the extracellular medium upon depolarization from treatment with veratridine (which prevents Na^+-channel closure) plus ouabain (which inhibits Na^+/K^+-ATPase; Fig. 6 a). Additionally, stable isotope tracing with uniformly labeled [$^{13}C_6$]glucose or [$^{13}C_5$] glutamine tracers revealed an altered composition of the released glutamate upon MPC inhibition, suggesting a shift away from mitochondrial glucose oxidation and toward that of glutamine/glutamate (Fig. 6 b). These data provide initial evidence that the glutamate pool oxidized during MPC inhibition is associated with the pool released upon depolarization.

Published March 2, 2017

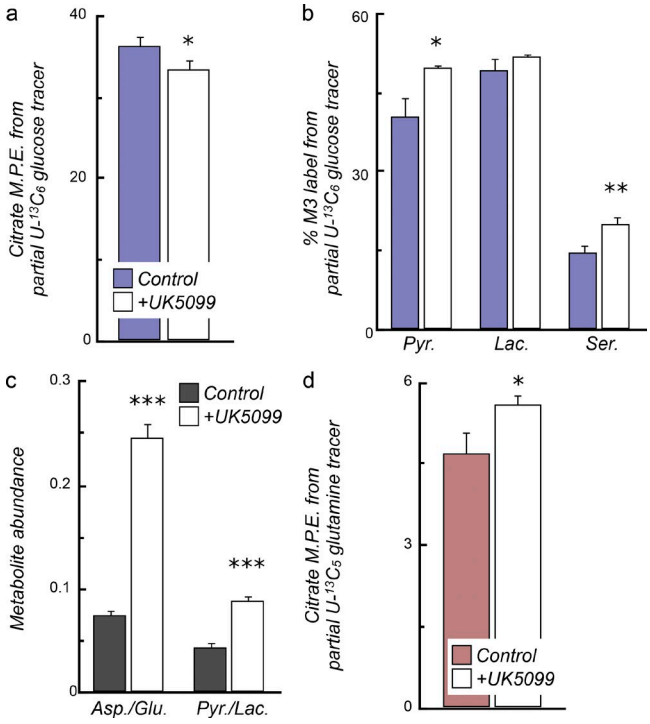

Figure 5. **Organotypic hippocampal slice cultures reproduce hallmarks of MPC inhibition.** (a) MPE of citrate from [U-$^{13}C_6$]glucose is decreased. (b) Increases in enrichment from a [U-$^{13}C_6$]glucose tracer are observed in fully labeled pyruvate and serine, but not lactate. Color scheme as in panel a. (c) Ratios of aspartate/glutamate and pyruvate/lactate in slice cultures are elevated. Metabolite ratios are internally normalized parameters and independent of the amount of starting material. (d) MPE of citrate from [U-$^{13}C_5$]glutamine is increased. All experiments were conducted in MEM as detailed in Materials and methods, with comparisons made between control conditions and 10 µM UK5099 treatment for 48 h. Data are $n = 6$ and presented as mean ± SEM. Asp., aspartate; Glu., glutamate; Lac., lactate; Pyr., pyruvate; Ser., serine. *, P < 0.05; **, P < 0.01; ***, P < 0.001.

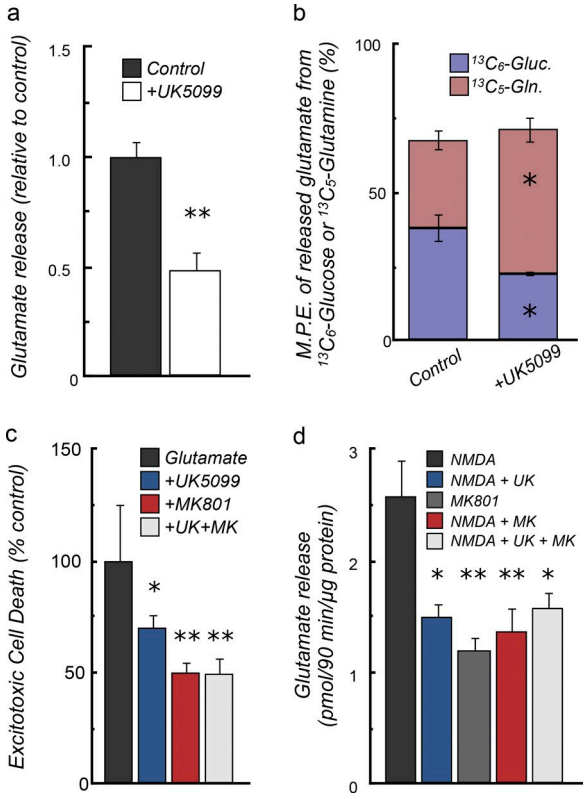

Figure 6. **UK5099 protects cortical neurons from excitotoxic injury by lowering the releasable glutamate pool.** (a) The relative amount of glutamate released upon depolarization from 25 µM veratridine with 1 µM ouabain is lowered upon MPC inhibition. (b) MPE from [U-$^{13}C_5$]glutamine (Gln.) and [U-$^{13}C_6$]glucose (Gluc.) into glutamate demonstrates that MPC inhibition can affect the composition of the glutamate pool released by veratridine/ouabain: enrichment from glucose decreases, whereas enrichment from glutamine increases after UK5099 treatment. Cells were treated with stable isotope tracers in Neuro-c lacking β-hydroxybutyrate. (c) MPC inhibition is protective from excitotoxic cell death in Neuro-c, measured 24 h after glutamate exposure. Protective effects from UK5099 are not additive to the protection afforded by the NMDA receptor antagonist MK801. (d) The quantity of glutamate released to the extracellular medium after 90-min treatment with 100 µM NMDA is reduced by UK5099. All data are $n = 4$ unless otherwise stated and presented as mean ± SEM. [UK5099], 10 µM for 24 h; MK801, 10 µM. *, P < 0.05; **, P < 0.01.

Because the data indicated that potentiating oxidation of glutamate can limit the size of the released pool, we hypothesized that MPC inhibition may protect from excitotoxic injury. Indeed, cortical neurons treated with UK5099 were protected from excitotoxic cell death in neuronal culture medium (Fig. 6 c). The protection afforded by pyruvate carrier inhibition was not additive to the protective effects of MK801, reinforcing that the mechanism of protection by MPC inhibition was mediated by the NMDA receptor. A similar profile of protection by UK5099 and MK801 was observed in assays conducted identically but lacking exogenously added glutamate (i.e., death induced only from the stress associated with fluid change during the assay; Fig. S4 a). This suggests that some excitotoxic death can be attributable to endogenous glutamate release and points to a spatio-temporal component within the neuronal population that contributes to the observed excitotoxicity. Although MK801 provided only ∼50% protection from excitotoxic death (Fig. 6 c), it is essential to note that conducting experiments in rich medium replete with several oxidizable substrates provides substantial protection over traditional assays in simple salts–based medium (Fig. S4 b). In fact, an ancillary finding of these experiments is that supplementing conventional, simple salts–based medium with nonglucose substrates provides protection during excitotoxicity (Fig. S4, c and d; Haces et al., 2008; Netzahualcoyotzi and Tapia, 2014).

The primary result that UK5099 protects from excitotoxic cell death informs a mechanism for the protective effects of pyruvate carrier inhibition: oxidation of the neuronal glutamate pool decreases the glutamate released to the extracellular space upon de-energization and limits the excitotoxic, positive feedback cascade. To test this concept and explicitly reveal a role for NMDA receptor–mediated depolarization, neurons were treated with 100 µM NMDA for a brief duration that evoked glutamate release but did not acutely compromise viability (Fig. S4, e and f). As expected, neurons treated with UK5099 released less glutamate to the extracellular space upon NMDA treatment, and this again was not additive to the effects of MK801 (Fig. 6 d).

Finally, to directly link MPC inhibition to reductions in the vesicular glutamate pool in presynaptic terminals, we conducted whole-cell patch-clamp recordings. The presynaptic, readily releasable glutamate pool was measured by recording postsynaptic currents while applying hypertonic sucrose-containing solution (500 mM for 4 s) to primary mouse cortical pyramidal neurons. Neurons treated with UK5099 exhibited a significantly

Published March 2, 2017

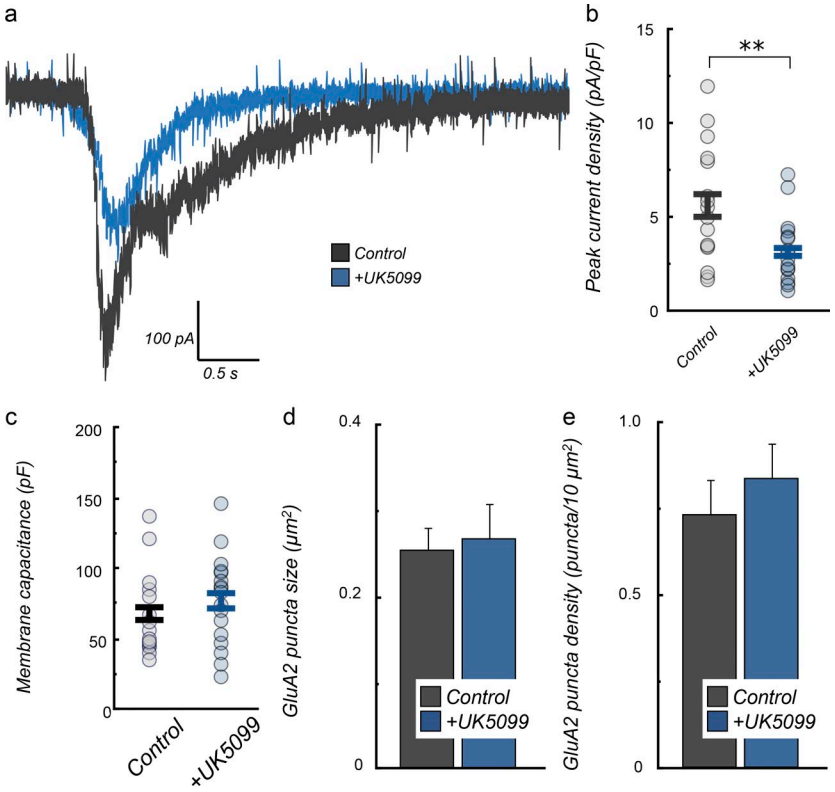

Figure 7. **Patch-clamp electrophysiology demonstrates that MPC inhibition reduces evoked glutamate release.** (a) Representative traces of EPSCs in response to hypertonic sucrose shock indicate decreased release of presynaptic glutamate. (b) Peak current density is lowered after 5 μM UK5099 treatment for 24 h. (c) Membrane capacitance after 5 μM UK5099 treatment for 24 h is unchanged. (d and e) Size (d) and density (e) of GluA2 puncta colocalized with vGlut1 are unchanged by UK5099 treatment. All data are $n \geq 16$ from three independent preparations and are presented as mean ± SEM. **, $P < 0.01$, by unpaired *t* test.

smaller peak current density in excitatory postsynaptic currents in response to sucrose shock (Fig. 7, a and b). Importantly, MPC inhibition did not significantly change either neuronal membrane capacitance (Fig. 7 c), reflecting unaltered cell membrane area, or synaptic density as measured by colocalization of postsynaptic α-amino-3-hydroxy-5-methyl-4-isoxazolepropionic acid receptors with presynaptic vesicular glutamate transporter 1 (vGlut1; Fig. 7, d and e; and Fig. S5). The electrophysiological data reinforce a model in which potentiating neuronal glutamate oxidation by MPC inhibition can attenuate the glutamate pool released upon depolarization (Fig. 8).

Discussion

Here we present evidence that TCA cycle metabolism and glutamatergic neurotransmission are linked via mitochondrial pyruvate uptake. The inarguable dependence of brain energy metabolism on arterial glucose is, of course, not mutually exclusive with neurons mobilizing glutamate as an oxidizable substrate. Glutamate is demonstrably de novo synthesized from glucose-derived carbon, and based on cellular context and metabolic demands, stored glutamate could be appropriated for either neurotransmission or oxidative metabolism. Of course, the data cannot exclude increased flux of other anaplerotic reactions to help compensate for MPC inhibition, most notably propionyl CoA production from valine or isoleucine. However, based on other cell types with comparable rates of BCAA oxidation (Green et al., 2016), such changes would likely be marginal relative to the substantive increase seen in glutamate oxidation.

A distinction should be drawn between the requirements for robust MPC activity during gestation and development as opposed to maturity. Homozygous knockout of either MPC paralog is embryonically lethal in mice (McCommis et al., 2015; Vanderperre et al., 2016), likely because of neurodevelopmental deficits (Vanderperre et al., 2016). After maturity, however, slight reductions in MPC activity could allow energy demands to be met while adjusting neurotransmitter balance. Indeed, a developmental requirement for a metabolic enzyme does not preclude its pharmacologic inhibition as a viable therapeutic strategy.

The context in which MPC inhibition would be beneficial is essential to its putative therapeutic value. In the healthy brain, substantial MPC inhibition could compromise cognitive

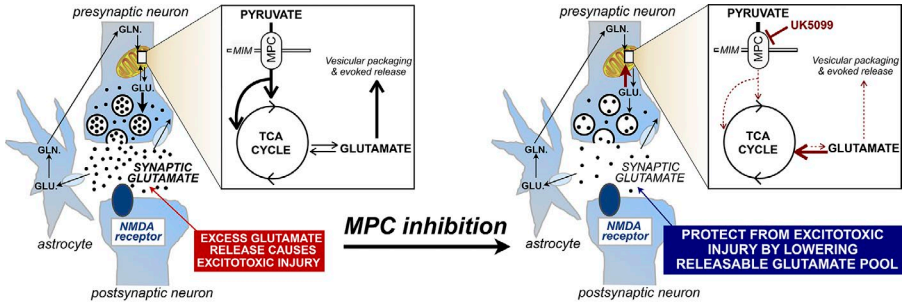

Figure 8. **The data support a model whereby pyruvate carrier inhibition increases glutamate oxidation to maintain energetics and anaplerosis.** This decreases the quantity of glutamate available for evoked release and can protect from excitotoxic cell death. GLN., glutamine; GLU., glutamate; MIM, mitochondrial inner membrane.

Published March 2, 2017

function, indicated by the fact that arterial glucose can drop to only ∼40% of normal levels before loss of consciousness (Cryer, 2007). Under pathological conditions such as ischemia, however, synaptic glutamate can increase by orders of magnitude within minutes (Rossi et al., 2000). Tonic levels of MPC inhibition may therefore protect from the excitotoxic sequelae of stroke by attenuating the synaptic glutamate concentration. Many efforts targeting excitatory amino acid receptors (e.g., potent NMDA receptor antagonists) have stalled because of prohibitory neurological side effects, exposing a need to explore alternative approaches to treat excitotoxicity (Lipton, 2004). Lowering synaptic glutamate by promoting its oxidation may provide a more forgiving approach that allows continued receptor function. In fact, weaker NMDA receptor antagonists such as memantine have far better clinical profiles than potent inhibitors such as MK801 (Lipton, 2004). Targeting mitochondrial pyruvate uptake to limit excitotoxic injury will likely involve the discovery of a novel class of MPC inhibitors, as current compounds are either nonspecific (Divakaruni et al., 2013; Du et al., 2013) or reactive nucleophiles such as UK5099 that are unattractive drug candidates (Hildyard et al., 2005). To that end, a thiazolidinedione that inhibits the MPC but exhibits reduced affinity toward peroxisome proliferator–activated receptor-γ has recently shown efficacy in several animal models of Parkinson's disease (Ghosh et al., 2016). Because endogenous regulators of mitochondrial pyruvate uptake have yet to be defined, the extent to which physiological regulation of MPC activity affects glutamatergic neurotransmission is currently unclear.

Speculatively, these results may also provide insight into the mechanism of how ketogenic diets can exert beneficial neurological effects, particularly with regard to medically refractory seizure disorders. Oxidation of ketone bodies cannot entirely compensate for reductions in brain glucose metabolism because they are not anaplerotic, so it is possible that neurotransmitter balance is adjusted in response to low-carbohydrate diets because of increased glutamate oxidation. Amino acid handling has been proposed as a means by which these diets are anticonvulsant (Yudkoff et al., 2008), although that study proposed a different mechanism whereby the presence of ketones increases flux of glutamate to GABA to control excitability via increased inhibitory signaling. Nonetheless, in vivo inhibition of seizures by a broad class of ionotropic glutamate receptor antagonists establishes a role for glutamate receptor overactivity in seizure disorders (Chapman, 2000). The metabolic pattern revealed here provides a strong foundation for in vivo testing of MPC inhibition to treat excitotoxic injury and, perhaps, suggests that the MPC may be a candidate target for a long-desired class of anticonvulsants that seek to pharmacologically mimic the benefits of the ketogenic diet (Masino and Rho, 2012).

Materials and methods

Animals and cell/tissue culture

All animal protocols were approved by the Institutional Animal Care and Use Committee of the University of California, San Diego. Cortical neurons were generated from embryonic day 18 Sprague-Dawley rats as described previously (Kushnareva et al., 2005). Cultures were ∼95% pure as determined by immunocytochemical staining to antineuronal nuclei or 200 kD antineurofilament. Cells were plated onto poly-D-lysine–coated wells of black-walled 96-well plates, Seahorse XF96 plates, or six-well dishes and maintained at 37°C in a humidified incubator with 5% CO_2. Cells for 96-well plate-based assays were seeded at 2.5×10^4 cells/well and maintained in maintenance medium composed of 200 µl Neurobasal (Thermo Fisher Scientific) medium supplemented with 1× B27 serum-free supplement (Thermo Fisher Scientific), 2 mM GlutaMAX (Thermo Fisher Scientific), 100 U/ml penicillin, and 100 µg/ml streptomycin. Cells in six-well dishes were seeded at 1.75×10^5 cells/well and maintained in 4 ml medium. Half the medium was replaced every 3–4 d. Experiments in 96-well plates were conducted at day in vitro (DIV) 13–17, and six-well dishes were used at 19–21 DIV. For electrophysiology, cortical cultures from FVB/N mice were prepared as previously described (except glutamine was replaced with GlutaMAX [Buren et al., 2016]), plated at 650 cells/mm^2, and used at DIV 17–18. Cortical astrocytes were prepared according to established methods (Kim and Magrané, 2011).

Organotypic hippocampal slice cultures were prepared as previously described (Stoppini et al., 1991) from postnatal day 6 Sprague-Dawley rats. After animals were anesthetized with isoflurane inhalation, cerebral hemispheres were quickly dissected in medium containing 218 mM sucrose, 4 mM KCl, 1.3 mM NaH_2PO_4, 5 mM $MgCl_2$, 1 mM $CaCl_2$, 26 mM $NaHCO_3$, 10 mM glucose, and 30 mM Hepes, pH 7.4. 300-µm hippocampal slices were generated using an automated tissue chopper (McIlwain) and transferred to slice culture medium composed of MEM (50-019; Corning) supplemented with 20% horse serum, 12.9 mM glucose, 1 mM glutamine, 2 mM $MgCl_2$, 1 mM $CaCl_2$, 0.07 mM ascorbic acid, 5.2 mM $NaHCO_3$, 30.5 mM Hepes, and 1 µg/ml insulin. Three slices were plated per cell culture insert (PICM03050; EMD Millipore) and fed with 0.75 ml culture medium. Medium was replaced every 2 d, and isotope tracers were added 12–14 d after preparation.

Viability

Viability was determined by measuring release of lactate dehydrogenase (LDH) in the extracellular medium after a given treatment (Cytotoxicity Detection kit #11-644-793-001; Roche; used according to manufacturer's instructions). Cell death was defined as the percentage of LDH activity associated with the assay medium relative to cell-associated activity. LDH activity was assessed with kinetic measurements over 5 min, and cell-associated LDH activity was determined by collecting medium after 30-min treatment with 2% (wt/vol) Triton X-100 to fully lyse cells.

Medium formulation

Custom Neuro-c (Table 1) used for studies with dissociated neuronal cultures was modeled after Neurobasal medium (Thermo Fisher Scientific) and purchased from ScienCell Research Laboratories. Neuro-c was composed with a base medium, to which additives were selectively included (Table 1) to a given experiment as indicated later.

Respirometry

Oxygen consumption measurements were made using a Seahorse XF96 or XFe96 Analyzer with a minimum of four biological replicates for each experiment and a minimum of five technical replicates per plate. Only the inner 60 wells of the 96-well plate were used for measurements; the outer rim was filled with 200 µl PBS before plating to minimize effects of temperature and evaporation during long-term incubation.

Permeabilized cells. Neurons were permeabilized with 3 nM recombinant, mutant perfringolysin O (PFO; XF PMP; Agilent Technologies; Divakaruni et al., 2013), offered specific substrates, and respiration was measured as previously described (Divakaruni et al., 2014b). Phosphorylating (state 3) respiration was measured in the presence of 4 mM ADP, and maximal respiration was measured after addition of 2 µM oligomycin and sequential additions of 2 µM FCCP. Rates were cor-

Published March 2, 2017

rected for background/nonmitochondrial respiration with addition of 1 µM rotenone and 1 µM antimycin A. Substrate concentrations are as follows: 5 mM pyruvate with 1 mM malate and 2 mM dichloroacetate (P/M); 5 mM glutamate with 5 mM malate (G/M); 10 mM succinate with 2 µM rotenone (S/R); 5 mM β-hydroxybutyrate with 1 mM malate (β-HB/M); 5 mM α-ketoisocaproate with 1 mM malate (KIC/M); 5 mM α-keto-β-methylvalerate with 1 mM malate (KMV/M); 5 mM α-ketoisovalerate with 1 mM malate (KIV/M); 1 mM malate (M); and 5 mM pyruvate with 1 mM malate, 2 mM dichloroacetate, and 25 mM methyl pyruvate (MePyr/M).

Intact cells. To measure the ability of respiration to acutely adapt to MPC inhibition (Fig. 2, b and c; and Fig. S2, b and c), maintenance medium was exchanged with Neuro-c (Table 1) supplemented with 5 mM Hepes, 8 mM glucose, and 1 mM pyruvate. Where indicated, medium was also supplemented with 3 mM β-hydroxybutyrate or 3 mM β-hydroxybutyrate plus 2 mM leucine. Cells were pretreated with UK5099 (3–300 nM) for 1 h. Respiration was measured under basal conditions as well as after injection of 2 µM oligomycin, two sequential additions of 250 nM FCCP, and 0.2 µM rotenone with 1 µM antimycin A.

When measuring the bioenergetic consequences of long-term UK5099 treatment (Fig. 3 b), it was necessary to conduct respirometry measurements under conditions closely matching those used for stable isotope tracing. Therefore, after treatment with UK5099 for 24 h, measurements were made with a Seahorse XFe Analyzer placed in a Coy Hypoxia Chamber (Coy Laboratory Products) with O_2 set to 21.7% (ambient) and CO_2 set to 5% to reproduce the environment of a cell culture incubator (Grassian et al., 2014). Maintenance medium was replaced with Neuro-c (Table 1) supplemented with 26.19 mM sodium bicarbonate, 2% (vol/vol) B27 supplement, 10.9 mM Hepes, 2 mM GlutaMAX, 0.8 mM leucine, 0.8 mM isoleucine, 0.8 mM valine, 8 mM glucose, 2 mM β-hydroxybutyrate, 0.22 mM pyruvate, and 0.02 mM phenol red. Rates were corrected for background/nonmitochondrial respiration with addition of 1 µM rotenone and 1 µM antimycin A.

Lactate efflux

Under conditions matching respirometry experiments for acute UK5099 treatment (Fig. 2 b), the extracellular medium was harvested, and lactate was quantified using an enzymatic assay as previously described (Mookerjee et al., 2015). In brief, sample medium was mixed 1:1 with a solution of 1 M Tris, pH 9.8, 20 mM EDTA, 400 mM hydrazine (309400; Sigma-Aldrich), 40 U/ml LDH (L3916; Sigma-Aldrich), and 4 mM NAD^+. The reaction velocity was measured after 2 min (340 nm excitation/460 emission), and values were calibrated against known lactate standards (L7022; Sigma-Aldrich).

ATP production rates

The ATP production rate was estimated as the sum of ATP produced from oxidative phosphorylation and glycolysis. The mitochondrial ATP production rate was estimated by multiplying the oligomycin-sensitive respiration rate by 5.45 (a P/O ratio of 2.73 [Brand, 2005; Watt et al., 2010], multiplied by 2 to convert rates from pmol O_2/min to pmol O/min). Because the rate of oligomycin-sensitive respiration will slightly overestimate the rate of proton leak-driven respiration (thereby underestimating the rate of ATP-linked respiration), a correction was made assuming a 10% overestimate of the proton leak rate (Affourtit and Brand, 2009). Glycolytic ATP production rates were calculated assuming a 1:1 stoichiometry between lactate efflux and ATP production (Divakaruni et al., 2014a). This will underestimate the actual rate, as it does not account for the glycolytic ATP produced during the formation of pyruvate that is ultimately diverted away from LDH and oxidized by mitochondria (Mookerjee et al., 2015).

Protein quantification

Cells were lysed with RIPA (50 mM Tris, pH 7.4, 150 mM NaCl, 1% [wt/vol] NP-40, 0.5% [wt/vol] sodium deoxycholate, and 0.1% [wt/vol] sodium dodecyl sulfate), and protein quantification was made using the bicinchoninic assay method (BCA protein assay kit; Thermo Fisher Scientific).

Stable isotope tracing

Cell culture and medium formulation for dissociated neuronal cultures. [U-$^{13}C_6$]glucose (CLM-1396), [U-$^{13}C_6$]leucine (CLM-2262), [U-$^{13}C_5$]glutamine (CLM-1822), and [3-$^{13}C_1$]glucose (CLM-1393) were purchased from Cambridge Isotope Laboratories. [U-$^{13}C_4$]β-hydroxybutyrate was purchased from Sigma-Aldrich (606030). When using a specific metabolic tracer, medium was formulated by replacing the substrate of interest with the isotopically labeled substrate while keeping all other substrates present and unlabeled. As glycolytic provision of pyruvate can be rate limiting in primary neural preparations (Choi et al., 2009), it was present at a low concentration in rich Neuro-c, but tracing with [$^{13}C_3$]pyruvate was not conducted because results would largely mimic studies with labeled glucose. Tracing was conducted in six-well dishes, with each well considered a technical replicate for a given preparation of neurons. Immediately before adding rich incubation medium for stable isotope tracing, maintenance medium was aspirated and cells were washed once with Neuro-c (Table 1) supplemented only with 26.19 mM sodium bicarbonate, 10.9 mM Hepes, and 0.02 mM phenol red before adding 2 ml of rich incubation medium containing stable isotope tracers. Wells were washed and treated individually, working very quickly to minimize the time neurons were exposed to air, and offered stable isotope tracers after one wash.

Treatment with stable isotope tracers. Rich incubation medium for stable isotope tracing was Neuro-c supplemented with the following: 26.19 mM sodium bicarbonate, 10.9 mM Hepes, 2 mM GlutaMAX, 100 U/ml penicillin, 100 µg/ml streptomycin, 8 mM glucose, 0.8 mM leucine, 0.8 mM isoleucine, 0.8 mM valine, 2 mM β-hydroxybutyrate, 0.22 mM pyruvate, B27 supplement, and 0.02 mM phenol red. 20 mM NaCl was added for an osmolarity similar to Neurobasal medium (Thermo Fisher Scientific). When tracing with labeled glutamine, GlutaMAX was omitted and replaced with 0.5 mM [U-$^{13}C_5$]glutamine, β-hydroxybutyrate was omitted, and 10 µM MK801 was added to prevent excitotoxic injury.

Metabolite extraction and gas chromatography/mass spectrometry analysis. Cells were treated with rich incubation medium containing stable isotope tracers for 24 h. At the conclusion of the experiment, 1 ml spent medium was set aside, spun to remove whole cells and debris, and kept at −80°C until analysis. The remaining medium was aspirated, and cells were washed with a 0.9% (wt/vol) NaCl solution. Polar metabolites and total fatty acids were extracted, derivatized, and analyzed as previously described (Vacanti et al., 2014). Ion fragments composed of ^{13}C atoms were quantified using gas chromatography/mass spectrometry. Isotope enrichment was designated as M0 (no ^{13}C atoms), M1 (one ^{13}C atom), M2 (two ^{13}C atoms), etc. Molar percent enrichment (MPE) of isotopes was calculated as the percentage of all atoms within the metabolite pool that are labeled:

$$\sum_{i=1}^{n} \frac{M_i \times i}{n},$$

where n is the number of carbon atoms in the metabolite and M_i is the relative abundance of the i-th mass isotopomer. To determine the percentage of newly synthesized palmitate after tracer addition and the relative contribution of different substrates to lipogenic AcCoA, isotopomer spectral analysis was conducted using INCA software as

Published March 2, 2017

Table 2. **Isotopomer spectral analysis**

Contribution to lipogenic AcCoA (%)	Description
AcM1.I (ab)→Ac (ab)	AcCoA containing one ^{13}C tracer label
AcM2.I (ab)→Ac (ab)	AcCoA containing two ^{13}C tracer labels
Ac.d (ab)→Ac (ab)	Unlabeled AcCoA
8*Ac (ab)→Palm.s (abcdefghijklmnop)	
De novo lipogenesis	
Palm.s→Palm	Newly synthesized palmitate
Palm.d→Palm	Preexisting (unlabeled) palmitate
0*Palm.s + 0*Palm.d→Palm.m	Mixing of pools for measurement

previously described (Metallo et al., 2011) and using the simplified network outlined in Table 2.

Tracing with organotypic hippocampal cultures. For organotypic hippocampal cultures, slice culture medium was made as described in Animals and cell/tissue culture but supplemented with either [U-$^{13}C_6$] glucose or [U-$^{13}C_5$]glutamine. As with tracing in dissociated cultures, all substrates were present during the experiments, and incorporation from either glucose or glutamine was measured by replacing unlabeled substrate with uniformly labeled substrate.

The powdered medium base is formulated with preexisting 5.6 mM glucose and 2 mM glutamine that could not be removed, so only a fraction of the total pool of glucose or glutamine was labeled for this work (12.9 mM of 18.5 mM total glucose was labeled; 1 mM of 3 mM total glutamine was labeled). 48 h after tracer incubation, slices were thoroughly washed with 0.9% saline, removed from the insert, wrapped in aluminum foil, and immediately snap-frozen in liquid nitrogen. Tissue was disrupted with a Precellys Evolution system (Bertin Technologies).

Glutamine uptake

Glutamine uptake, calculated as the difference in concentration in the extracellular medium after 24 h, was assessed using a 2950 Biochemistry Analyzer (YSI).

Excitotoxicity

Glutamate excitotoxicity experiments were conducted in either a simple salts–based medium (Fig. S4, b–d) or customized Neuro-c (Fig. 6 c), and fluid changes and additions were made as quickly as possible to minimize exposure to air. For experiments conducted in salt-based medium, maintenance medium (Neurobasal + B27, GlutaMAX, and penicillin/streptomycin) was replaced with 50 µl HBSS (137 mM NaCl, 5 mM KCl, 10 mM $NaHCO_3$, 20 mM Hepes, 0.6 mM KH_2PO_4, 1.4 mM $CaCl_2$, 0.9 mM $MgSO_4$, 10 mM glucose, and 1 mM pyruvate) with or without 100 µM glutamate and 10 µM glycine. Where indicated, medium was supplemented with 2 mM β-hydroxybutyrate and 2 mM leucine with or without 30 nM UK5099 (the HBSS medium for UK5099 treatment did not contain albumin). After a 30-min incubation at 37°C, 150 µl of maintenance medium was added, and cells were incubated for 24 h before assessment of viability. Excitotoxic cell death was calculated as the difference in viability between groups with and without glutamate/glycine present in HBSS.

For experiments in customized Neuro-c, the medium composition matched the incubation medium used for stable isotope tracing. For measurements of excitotoxicity, maintenance medium was replaced with 100 µl supplemented Neuro-c medium with or without glutamate (500 µM). UK5099 (10 µM; medium contains B27 supplement with albumin), MK801 (10 µM), or both were added 30 min before glutamate addition. Cells were incubated for 24 h before assessment of viability. Excitotoxic cell death (Fig. 6 c) was calculated as the difference in viability between groups with and without glutamate present in the medium. For all excitotoxicity experiments, four biological replicates were conducted for each experiment with five technical replicates per plate.

Glutamate release and quantification

Glutamate release assays (Figs. 6 d and S4 f) were conducted in 96-well plates. 24 h before the experiment, maintenance medium was replaced with 200 µl incubation medium with the same composition used for stable isotope tracing. Neurons were treated with or without 10 µM UK5099 for this period. Medium was then exchanged for fresh incubation medium (groups containing 10 µM MK801 were pretreated for 30 min) with or without 100 µM NMDA for 90 min. Medium was then harvested, spun to remove debris, and analyzed using a commercially available, Amplex red–based detection assay calibrated against glutamate standards (A12221; Thermo Fisher Scientific). To determine the total releasable pool of cytoplasmic glutamate, cells in separate wells were permeabilized with the recombinant, mutant cytolysin PFO (3 nM) to release cytoplasmic contents. Matched plates were used with an identical treatment scheme to determine effects of treatment on viability using the LDH release assay.

For glutamate release assays to be analyzed by gas chromatography/mass spectrometry (Fig. 6, a and b), six-well dishes of neuronal cultures were treated similarly to other isotopic tracer experiments using [U-$^{13}C_5$]glutamine. After quickly washing cells with 0.9% NaCl, neurons were depolarized by treatment with 25 µM veratridine plus 1 µM ouabain in artificial cerebrospinal fluid composed of 120 mM NaCl, 3.5 mM KCl, 1.3 mM $CaCl_2$, 0.04 mM KH_2PO_4, 1 mM $MgCl_2$, 5 mM Hepes, and 8 mM glucose. After 90 min, the medium was collected, centrifuged to remove any debris, and analyzed. Norvaline was used as an internal standard, and low phosphate was used to avoid potential complications with MS analysis.

Quantification of intracellular glutamate (Fig. S2 c) was made using an Amplex Red–based detection assay calibrated against glutamate standards (A12221; Thermo Fisher Scientific). After 24 h with or without UK5099 treatment, cells were scraped and pelleted after washing, disrupted by repeated freeze-thaw cycles in hypotonic PBS with 10 nM recombinant, mutant PFO, and kept at −80°C until analysis.

Electrophysiology

At 13–18 DIV, half of the maintenance medium was replaced with new maintenance medium supplemented with 4 mM β-hydroxybutyrate and either 10 µM UK5099 or a DMSO vehicle control (final concentrations of 2 mM β-hydroxybutyrate and 5 µM UK5099). Cultures were treated for at least 24 h before coverslips were placed in a recording chamber perfused with external bath solution of artificial cerebrospinal fluid (pH 7.3, 310–320 mOsm) composed of 167 mM NaCl, 2.4 mM KCl, 2 mM $CaCl_2$, 1 mM $MgCl_2$, 10 mM Hepes, 10 mM glucose, 1 mM pyruvate, 2 mM β-hydroxybutyrate, 2 mM leucine, 100 µM picrotoxin (to inhibit GABAergic transmission), and 0.3 µM tetrodotoxin (to inhibit neuronal action potentials).

To measure the size of the presynaptic readily releasable pool (Rosenmund and Stevens, 1996; Buren et al., 2016), 500 mM sucrose prepared in the external bath solution was applied for 4 s through a theta tube closely apposed to the recorded cell. Whole-cell patch-clamp recordings were conducted under voltage clamp at −70mV using an Axopatch 200B amplifier (Axon Instruments) and pClamp 10.2 software (Molecular Devices). Cortical pyramidal neurons were selected by morphology for recording. Glass recording electrodes (3–6 MΩ) contained internal solution prepared with 145 mM K^+-gluconate, 1 mM

Published March 2, 2017

$MgCl_2$, 10 mM Hepes, 1 mM EGTA, 2 mM Mg^{2+}-ATP, and 0.5 mM Na^+-GTP (pH 7.3, 280 mOsm). The access resistance (R_a) was typically 10–20 MΩ, and recordings were rejected if R_a exceeded 25 MΩ. Traces were analyzed with Clampfit 10.2 (Molecular Devices).

Immunostaining of GluA2

To examine whether α-amino-3-hydroxy-5-methyl-4-isoxazolepropionic acid receptor expression or distribution was altered by UK5099 treatment, three to six coverslips from each preparation of neurons were fixed in 4% PFA and 4% sucrose for 15 min and washed with 0.03% Triton X-100 (Sigma-Aldrich) in PBS (PBST). Cells were then incubated in methanol at −20°C for permeabilization, washed twice with PBST before blocking with 10% normal goat serum for 45 min at RT, and then incubated in primary antibodies overnight at 4°C (mouse anti-GluA2 [1:500; MAB397; EMD Millipore] and guinea pig anti-vGlut1 [1:4,000, AB5905; EMD Millipore] in 2% normal goat serum PBST).

Cultures were washed three times with PBST before incubation with secondary antibodies at RT for 2 h (goat anti–mouse Alexa Fluor 568 [1:1,000, A11031; Invitrogen] and donkey anti–guinea pig AMCA [1:200, 706-155-148; Jackson ImmunoResearch Laboratories, Inc.]). Cells were then washed with PBST and mounted with Fluoromount-G (0100-01; SouthernBiotech) on micro slides (2948-75X25; Corning). Images were taken under 63× oil lenses (1.4 NA) with an Axiovert 200 M epifluorescence microscope (ZEISS) and ZEN 2012 software. Dendrites were visualized with GluA2 staining, which stains both internal and surface GluA2 proteins. Seven to 15 images in the *z*-plane were acquired per cell, focusing on the dendritic tree, and the best-focused image planes were selected and exported as TIFF files. Two or three regions of interest on the dendritic tree in each image were selected in ImageJ 1.50a software and manually thresholded to remove background by adjusting the brightness and contrast for both GluA2 and vGlut1 channels. Only GluA2 puncta colocalized with vGlut1 were selected for measurement of size and density using ImageJ.

Statistics

All statistical analysis was conducted with GraphPad Prism 5.0 using, where appropriate, either analysis of variance (repeated-measures with Dunnett's post hoc test) or a paired, two-way Student's *t* test. Where appropriate, statistics were calculated on the square root of normalized data.

Online supplemental material

Fig. S1 shows that primary cortical neurons exhibit metabolic flexibility. Fig. S2 shows that inhibition of mitochondrial pyruvate uptake can adjust the abundance and composition of the neuronal glutamate pool while maintaining metabolic rates. Fig. S3 shows glutamine/glutamate oxidation is preferentially increased upon neuronal MPC inhibition. Fig. S4 shows that adjusting neuronal substrate metabolism can protect from glutamate excitotoxicity. Fig.S5 shows that UK5099 treatment does not compromise synaptic density.

Acknowledgments

This work was supported by National Institutes of Health grants R01NS087611 (A.N. Murphy) and R01CA188652 (C.M. Metallo), Teva Pharmaceuticals (I.J. Reynolds and A.N. Murphy), Seahorse Bioscience (A.S. Divakaruni and A.N. Murphy), Searle Scholar Awards (C.M. Metallo and B.L. Bloodgood), National Science Foundation Career Award (#1454425 to C.M. Metallo), and Canadian Institutes of Health Research operating grant (FDN-143210 to L.A. Raymond). A.N. Murphy and A.S. Divakaruni have been supported by funding from Teva Pharmaceuticals and Seahorse Bioscience. I.J. Reynolds is an employee of Teva Pharmaceuticals.

The authors declare no additional competing financial interests.

Author contributions: A.S. Divakaruni and A.N. Murphy conceived the project. A.S. Divakaruni, M. Wallace, C. Buren, E. Li, and A.N. Murphy carried out the experiments. A.S. Divakaruni, M. Wallace, C. Buren, I.J. Reynolds, B.L. Bloodgood, L.A. Raymond, C.M. Metallo, and A.N. Murphy designed the experiments and interpreted the data. K. Martyniuk, A.Y. Andreyev, J.A. Fields, and T. Cordes provided expert technical assistance. A.S. Divakaruni and A.N. Murphy wrote the manuscript with editing and approval from all authors.

Submitted: 15 December 2016
Revised: 6 January 2017
Accepted: 9 January 2017

References

Affourtit, C., and M.D. Brand. 2009. Measuring mitochondrial bioenergetics in INS-1E insulinoma cells. *Methods Enzymol.* 457:405–424. http://dx.doi.org/10.1016/S0076-6879(09)05023-X

Bélanger, M., I. Allaman, and P.J. Magistretti. 2011. Brain energy metabolism: Focus on astrocyte-neuron metabolic cooperation. *Cell Metab.* 14:724–738. http://dx.doi.org/10.1016/j.cmet.2011.08.016

Brand, M.D. 2005. The efficiency and plasticity of mitochondrial energy transduction. *Biochem. Soc. Trans.* 33:897–904. http://dx.doi.org/10.1042/BST0330897

Bricker, D.K., E.B. Taylor, J.C. Schell, T. Orsak, A. Boutron, Y.-C. Chen, J.E. Cox, C.M. Cardon, J.G. Van Vranken, N. Dephoure, et al. 2012. A mitochondrial pyruvate carrier required for pyruvate uptake in yeast, *Drosophila*, and humans. *Science.* 337:96–100. http://dx.doi.org/10.1126/science.1218099

Buren, C., M.P. Parsons, A. Smith-Dijak, and L.A. Raymond. 2016. Impaired development of cortico-striatal synaptic connectivity in a cell culture model of Huntington's disease. *Neurobiol. Dis.* 87:80–90. http://dx.doi.org/10.1016/j.nbd.2015.12.009

Chapman, A.G. 2000. Glutamate and epilepsy. *J. Nutr.* 130:1043S–1045S.

Chinopoulos, C. 2013. Which way does the citric acid cycle turn during hypoxia? The critical role of α-ketoglutarate dehydrogenase complex. *J. Neurosci. Res.* 91:1030–1043. http://dx.doi.org/10.1002/jnr.23196

Choi, D.W., and S.M. Rothman. 1990. The role of glutamate neurotoxicity in hypoxic-ischemic neuronal death. *Annu. Rev. Neurosci.* 13:171–182. http://dx.doi.org/10.1146/annurev.ne.13.030190.001131

Choi, S.W., A.A. Gerencser, and D.G. Nicholls. 2009. Bioenergetic analysis of isolated cerebrocortical nerve terminals on a microgram scale: Spare respiratory capacity and stochastic mitochondrial failure. *J. Neurochem.* 109:1179–1191. http://dx.doi.org/10.1111/j.1471-4159.2009.06055.x

Clarke, D.D., and L. Sokoloff. 1994. Circulation and energy metabolism of the brain. *In* Basic Neurochemistry. Fifth Edition. G.J. Siegel, B.W. Agranoff, R.W. Albers, and P.B. Molinoff, editors. Raven Press, New York. 645–680.

Coyle, J.T., and P. Puttfarcken. 1993. Oxidative stress, glutamate, and neurodegenerative disorders. *Science.* 262:689–695. http://dx.doi.org/10.1126/science.7901908

Craft, S. 2012. Alzheimer disease: Insulin resistance and AD—extending the translational path. *Nat. Rev. Neurol.* 8:360–362. http://dx.doi.org/10.1038/nrneurol.2012.112

Cryer, P.E. 2007. Hypoglycemia, functional brain failure, and brain death. *J. Clin. Invest.* 117:868–870. http://dx.doi.org/10.1172/JCI31669

Cunnane, S., S. Nugent, M. Roy, A. Courchesne-Loyer, E. Croteau, S. Tremblay, A. Castellano, F. Pifferi, C. Bocti, N. Paquet, et al. 2011. Brain fuel metabolism, aging, and Alzheimer's disease. *Nutrition.* 27:3–20. http://dx.doi.org/10.1016/j.nut.2010.07.021

Daikhin, Y., and M. Yudkoff. 2000. Compartmentation of brain glutamate metabolism in neurons and glia. *J. Nutr.* 130(4S, Suppl):1026S–1031S.

DeBerardinis, R.J., and T. Cheng. 2010. Q's next: The diverse functions of glutamine in metabolism, cell biology and cancer. *Oncogene.* 29:313–324. http://dx.doi.org/10.1038/onc.2009.358

de la Monte, S.M. 2012. Brain insulin resistance and deficiency as therapeutic targets in Alzheimer's disease. *Curr. Alzheimer Res.* 9:35–66. http://dx.doi.org/10.2174/156720512799015037

Divakaruni, A.S., S.E. Wiley, G.W. Rogers, A.Y. Andreyev, S. Petrosyan, M. Loviscach, E.A. Wall, N. Yadava, A.P. Heuck, D.A. Ferrick, et al. 2013. Thiazolidinediones are acute, specific inhibitors of the mitochondrial pyruvate carrier. *Proc. Natl. Acad. Sci. USA.* 110:5422–5427. http://dx.doi.org/10.1073/pnas.1303360110

Divakaruni, A.S., A. Paradyse, D.A. Ferrick, A.N. Murphy, and M. Jastroch. 2014a. Analysis and interpretation of microplate-based oxygen consumption and pH data. *Methods Enzymol.* 547:309–354. http://dx.doi.org/10.1016/B978-0-12-801415-8.00016-3

Divakaruni, A.S., G.W. Rogers, and A.N. Murphy. 2014b. Measuring mitochondrial function in permeabilized cells using the Seahorse XF analyzer or a Clark-type oxygen electrode. *Curr. Protoc. Toxicol.* 60:1–16. https://doi.org/10.1002/0471140856.tx2502s60

Du, J., W.M. Cleghorn, L. Contreras, K. Lindsay, A.M. Rountree, A.O. Chertov, S.J. Turner, A. Sahaboglu, J. Linton, M. Sadilek, et al. 2013. Inhibition of mitochondrial pyruvate transport by zaprinast causes massive accumulation of aspartate at the expense of glutamate in the retina. *J. Biol. Chem.* 288:36129–36140. http://dx.doi.org/10.1074/jbc.M113.507285

Fillmore, N., and G.D. Lopaschuk. 2013. Targeting mitochondrial oxidative metabolism as an approach to treat heart failure. *Biochim. Biophys. Acta.* 1833:857–865. http://dx.doi.org/10.1016/j.bbamcr.2012.08.014

Gähwiler, B.H., M. Capogna, D. Debanne, R.A. McKinney, and S.M. Thompson. 1997. Organotypic slice cultures: A technique has come of age. *Trends Neurosci.* 20:471–477. http://dx.doi.org/10.1016/S0166-2236(97)01122-3

Ghosh, A., T. Tyson, S. George, E.N. Hildebrandt, J.A. Steiner, Z. Madaj, E. Schulz, E. Machiela, W.G. McDonald, M.L. Escobar Galvis, et al. 2016. Mitochondrial pyruvate carrier regulates autophagy, inflammation, and neurodegeneration in experimental models of Parkinson's disease. *Sci. Transl. Med.* 8:368ra174. http://dx.doi.org/10.1126/scitranslmed.aag2210

Giménez-Cassina, A., J.R. Martínez-François, J.K. Fisher, B. Szlyk, K. Polak, J. Wiwczar, G.R. Tanner, A. Lutas, G. Yellen, and N.N. Danial. 2012. BAD-dependent regulation of fuel metabolism and $K(_{ATP})$ channel activity confers resistance to epileptic seizures. *Neuron.* 74:719–730. http://dx.doi.org/10.1016/j.neuron.2012.03.032

Grassian, A.R., S.J. Parker, S.M. Davidson, A.S. Divakaruni, C.R. Green, X. Zhang, K.L. Slocum, M. Pu, F. Lin, C. Vickers, et al. 2014. IDH1 mutations alter citric acid cycle metabolism and increase dependence on oxidative mitochondrial metabolism. *Cancer Res.* 74:3317–3331. http://dx.doi.org/10.1158/0008-5472.CAN-14-0772-T

Gray, L.R., M.R. Sultana, A.J. Rauckhorst, L. Oonthonpan, S.C. Tompkins, A. Sharma, X. Fu, R. Miao, A.D. Pewa, K.S. Brown, et al. 2015. Hepatic mitochondrial pyruvate carrier 1 is required for efficient regulation of gluconeogenesis and whole-body glucose homeostasis. *Cell Metab.* 22:669–681. http://dx.doi.org/10.1016/j.cmet.2015.07.027

Green, C.R., M. Wallace, A.S. Divakaruni, S.A. Phillips, A.N. Murphy, T.P. Ciaraldi, and C.M. Metallo. 2016. Branched-chain amino acid catabolism fuels adipocyte differentiation and lipogenesis. *Nat. Chem. Biol.* 12:15–21. http://dx.doi.org/10.1038/nchembio.1961

Haces, M.L., K. Hernández-Fonseca, O.N. Medina-Campos, T. Montiel, J. Pedraza-Chaverri, and L. Massieu. 2008. Antioxidant capacity contributes to protection of ketone bodies against oxidative damage induced during hypoglycemic conditions. *Exp. Neurol.* 211:85–96. http://dx.doi.org/10.1016/j.expneurol.2007.12.029

Hartman, A.L., M. Gasior, E.P. Vining, and M.A. Rogawski. 2007. The neuropharmacology of the ketogenic diet. *Pediatr. Neurol.* 36:281–292. http://dx.doi.org/10.1016/j.pediatrneurol.2007.02.008

Hassel, B. 2001. Pyruvate carboxylation in neurons. *J. Neurosci. Res.* 66:755–762. http://dx.doi.org/10.1002/jnr.10044

Herzig, S., E. Raemy, S. Montessuit, J.-L. Veuthey, N. Zamboni, B. Westermann, E.R.S. Kunji, and J.-C. Martinou. 2012. Identification and functional expression of the mitochondrial pyruvate carrier. *Science.* 337:93–96. http://dx.doi.org/10.1126/science.1218530

Hildyard, J.C., C. Ammälä, I.D. Dukes, S.A. Thomson, and A.P. Halestrap. 2005. Identification and characterisation of a new class of highly specific and potent inhibitors of the mitochondrial pyruvate carrier. *Biochim. Biophys. Acta.* 1707:221–230. http://dx.doi.org/10.1016/j.bbabio.2004.12.005

Johri, A., and M.F. Beal. 2012. Mitochondrial dysfunction in neurodegenerative diseases. *J. Pharmacol. Exp. Ther.* 342:619–630. http://dx.doi.org/10.1124/jpet.112.192138

Kajimoto, M., D.B. Atkinson, D.R. Ledee, E.-B. Kayser, P.G. Morgan, M.M. Sedensky, N.G. Isern, C. Des Rosiers, and M.A. Portman. 2014. Propofol compared with isoflurane inhibits mitochondrial metabolism in immature swine cerebral cortex. *J. Cereb. Blood Flow Metab.* 34:514–521. http://dx.doi.org/10.1038/jcbfm.2013.229

Kelley, D.E. 2005. Skeletal muscle fat oxidation: Timing and flexibility are everything. *J. Clin. Invest.* 115:1699–1702. http://dx.doi.org/10.1172/JCI25758

Kim, H.J., and J. Magrané. 2011. Isolation and culture of neurons and astrocytes from the mouse brain cortex. *Methods Mol. Biol.* 793:63–75. http://dx.doi.org/10.1007/978-1-61779-328-8_4

Kushnareva, Y.E., S.E. Wiley, M.W. Ward, A.Y. Andreyev, and A.N. Murphy. 2005. Excitotoxic injury to mitochondria isolated from cultured neurons. *J. Biol. Chem.* 280:28894–28902. http://dx.doi.org/10.1074/jbc.M503090200

Lipton, S.A. 2004. Failures and successes of NMDA receptor antagonists: Molecular basis for the use of open-channel blockers like memantine in the treatment of acute and chronic neurologic insults. *NeuroRx.* 1:101–110. http://dx.doi.org/10.1602/neurorx.1.1.101

Lund, T.M., O. Risa, U. Sonnewald, A. Schousboe, and H.S. Waagepetersen. 2009. Availability of neurotransmitter glutamate is diminished when beta-hydroxybutyrate replaces glucose in cultured neurons. *J. Neurochem.* 110:80–91. http://dx.doi.org/10.1111/j.1471-4159.2009.06115.x

Lutas, A., and G. Yellen. 2013. The ketogenic diet: Metabolic influences on brain excitability and epilepsy. *Trends Neurosci.* 36:32–40. http://dx.doi.org/10.1016/j.tins.2012.11.005

Maragakis, N.J., and J.D. Rothstein. 2001. Glutamate transporters in neurologic disease. *Arch. Neurol.* 58:365–370. http://dx.doi.org/10.1001/archneur.58.3.365

Marin-Valencia, I., C. Yang, T. Mashimo, S. Cho, H. Baek, X.-L. Yang, K.N. Rajagopalan, M. Maddie, V. Vemireddy, Z. Zhao, et al. 2012. Analysis of tumor metabolism reveals mitochondrial glucose oxidation in genetically diverse human glioblastomas in the mouse brain in vivo. *Cell Metab.* 15:827–837. http://dx.doi.org/10.1016/j.cmet.2012.05.001

Masino, S.A., and J.M. Rho. 2012. Mechanisms of ketogenic diet action. *In* Jasper's Basic Mechanisms of the Epilepsies. Fourth edition. J.L. Noebls, M. Avoli, M.A. Rogawski, R.W. Olsen, and A.V. Delgado-Escueta, editors. National Center for Biotechnology Information, USA, Bethesda, MD. 1–35. http://dx.doi.org/10.1093/med/9780199746545.003.0078

McCommis, K.S., Z. Chen, X. Fu, W.G. McDonald, J.R. Colca, R.F. Kletzien, S.C. Burgess, and B.N. Finck. 2015. Loss of mitochondrial pyruvate carrier 2 in the liver leads to defects in gluconeogenesis and compensation via pyruvate-alanine cycling. *Cell Metab.* 22:682–694. http://dx.doi.org/10.1016/j.cmet.2015.07.028

McKenna, M.C., C.A. Dienel, U. Sonnewald, H.S. Waagepetersen, and A. Schousboe. 2012. Energy metabolism of the brain. *In* Basic Neurochemistry: Principles of Molecular, Cellular, and Medical Neurobiology. Eighth Edition. S. Brady, G. Siegel, R.W. Albers, and D. Price, editors. Academic Press, New York. 200–231. http://dx.doi.org/10.1016/B978-0-12-374947-5.00011-0

Meldrum, B.S. 2000. Glutamate as a neurotransmitter in the brain: Review of physiology and pathology. *J. Nutr.* 130:1007S–1015S.

Metallo, C.M., P.A. Gameiro, E.L. Bell, K.R. Mattaini, J. Yang, K. Hiller, C.M. Jewell, Z.R. Johnson, D.J. Irvine, L. Guarente, et al. 2011. Reductive glutamine metabolism by IDH1 mediates lipogenesis under hypoxia. *Nature.* 481:380–384. https://doi.org/10.1038/nature10602

Mookerjee, S.A., R.L. Goncalves, A.A. Gerencser, D.G. Nicholls, and M.D. Brand. 2015. The contributions of respiration and glycolysis to extracellular acid production. *Biochim. Biophys. Acta.* 1847:171–181. http://dx.doi.org/10.1016/j.bbabio.2014.10.005

Muoio, D.M. 2014. Metabolic inflexibility: When mitochondrial indecision leads to metabolic gridlock. *Cell.* 159:1253–1262. http://dx.doi.org/10.1016/j.cell.2014.11.034

Netzahualcoyotzi, C., and R. Tapia. 2014. Energy substrates protect hippocampus against endogenous glutamate-mediated neurodegeneration in awake rats. *Neurochem. Res.* 39:1346–1354. http://dx.doi.org/10.1007/s11064-014-1318-y

Nicholls, D.G. 2009. Spare respiratory capacity, oxidative stress and excitotoxicity. *Biochem. Soc. Trans.* 37:1385–1388. http://dx.doi.org/10.1042/BST0371385

Olson, K.A., J.C. Schell, and J. Rutter. 2016. Pyruvate and metabolic flexibility: Illuminating a path toward selective cancer therapies. *Trends Biochem. Sci.* 41:219–230. http://dx.doi.org/10.1016/j.tibs.2016.01.002

Pavlova, N.N., and C.B. Thompson. 2016. The emerging hallmarks of cancer metabolism. *Cell Metab.* 23:27–47. http://dx.doi.org/10.1016/j.cmet.2015.12.006

Rosenmund, C., and C.F. Stevens. 1996. Definition of the readily releasable pool of vesicles at hippocampal synapses. *Neuron.* 16:1197–1207. http://dx.doi.org/10.1016/S0896-6273(00)80146-4

Rossi, D.J., T. Oshima, and D. Attwell. 2000. Glutamate release in severe brain ischaemia is mainly by reversed uptake. *Nature.* 403:316–321. http://dx.doi.org/10.1038/35002090

Schousboe, A., L.K. Bak, and H.S. Waagepetersen. 2013. Astrocytic control of biosynthesis and turnover of the neurotransmitters glutamate and GABA. *Front. Endocrinol. (Lausanne).* 4:102. https://doi.org/10.3389/fendo.2013.00102

Stanley, I.A., S.M. Ribeiro, A. Giménez-Cassina, E. Norberg, and N.N. Danial. 2014. Changing appetites: The adaptive advantages of fuel choice. *Trends Cell Biol.* 24:118–127. http://dx.doi.org/10.1016/j.tcb.2013.07.010

Stoppini, L., P.A. Buchs, and D. Muller. 1991. A simple method for organotypic cultures of nervous tissue. *J. Neurosci. Methods.* 37:173–182. http://dx.doi.org/10.1016/0165-0270(91)90128-M

Szydlowska, K., and M. Tymianski. 2010. Calcium, ischemia and excitotoxicity. *Cell Calcium.* 47:122–129. http://dx.doi.org/10.1016/j.ceca.2010.01.003

Tardito, S., A. Oudin, S.U. Ahmed, F. Fack, O. Keunen, L. Zheng, H. Miletic, P.Ø. Sakariassen, A. Weinstock, A. Wagner, et al. 2015. Glutamine synthetase activity fuels nucleotide biosynthesis and supports growth of glutamine-restricted glioblastoma. *Nat. Cell Biol.* 17:1556–1568. http://dx.doi.org/10.1038/ncb3272

Tennant, D.A., R.V. Durán, and E. Gottlieb. 2010. Targeting metabolic transformation for cancer therapy. *Nat. Rev. Cancer.* 10:267–277. http://dx.doi.org/10.1038/nrc2817

Vacanti, N.M., A.S. Divakaruni, C.R. Green, S.J. Parker, R.R. Henry, T.P. Ciaraldi, A.N. Murphy, and C.M. Metallo. 2014. Regulation of substrate utilization by the mitochondrial pyruvate carrier. *Mol. Cell.* 56:425–435. http://dx.doi.org/10.1016/j.molcel.2014.09.024

Vanderperre, B., S. Herzig, P. Krznar, M. Hörl, Z. Ammar, S. Montessuit, S. Pierredon, N. Zamboni, and J.-C. Martinou. 2016. Embryonic lethality of mitochondrial pyruvate carrier 1 deficient mouse can be rescued by a ketogenic diet. *PLoS Genet.* 12:e1006056. http://dx.doi.org/10.1371/journal.pgen.1006056

Watt, I.N., M.G. Montgomery, M.J. Runswick, A.G.W. Leslie, and J.E. Walker. 2010. Bioenergetic cost of making an adenosine triphosphate molecule in animal mitochondria. *Proc. Natl. Acad. Sci. USA.* 107:16823–16827. http://dx.doi.org/10.1073/pnas.1011099107

Yang, C., B. Ko, C.T. Hensley, L. Jiang, A.T. Wasti, J. Kim, J. Sudderth, M.A. Calvaruso, L. Lumata, M. Mitsche, et al. 2014. Glutamine oxidation maintains the TCA cycle and cell survival during impaired mitochondrial pyruvate transport. *Mol. Cell.* 56:414–424. http://dx.doi.org/10.1016/j.molcel.2014.09.025

Yudkoff, M., Y. Daikhin, O. Horyn, I. Nissim, and I. Nissim. 2008. Ketosis and brain handling of glutamate, glutamine, and GABA. *Epilepsia.* 49(Suppl 8):73–75. http://dx.doi.org/10.1111/j.1528-1167.2008.01841.x

Divakaruni et al., https://doi.org/10.1083/jcb.201612067

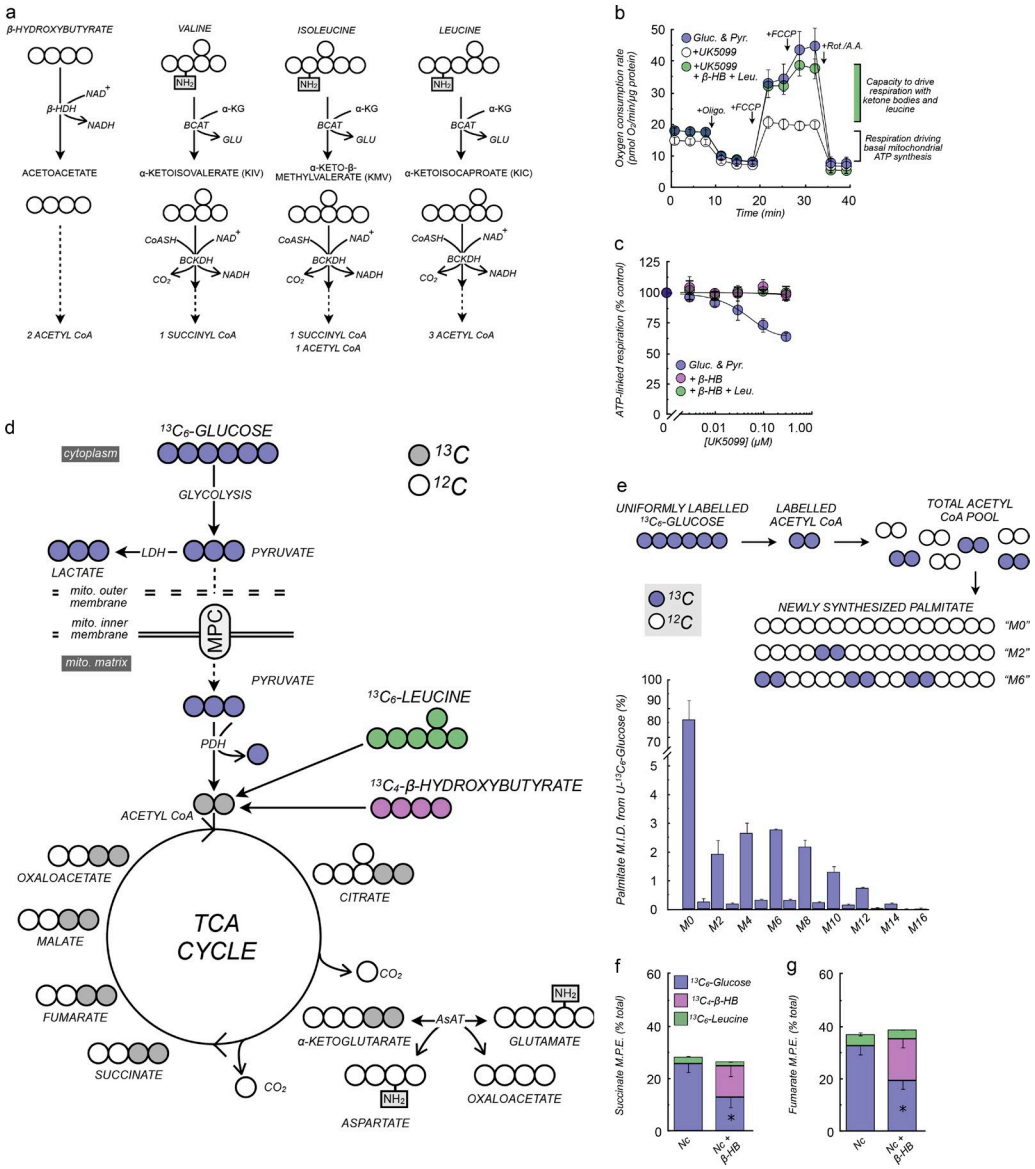

Figure S1. **Metabolic flexibility in primary cortical neurons.** (a) Oxidation of the ketone body β-hydroxybutyrate generates NADH via β-hydroxybutyrate dehydrogenase (β-HDH) and ultimately produces two acetyl CoA molecules. All branched-chain amino acids are deamidated by the branched-chain aminotransferase (BCAT), and oxidation of the resulting keto acid generates NADH via the branched chain keto acid dehydrogenase (BCKDH). α-KG, α-ketoglutarate. (b) Sample kinetic trace of oxygen consumption shows the capacity of neurons to use nonglucose substrates to fuel respiration. The respiration used to drive basal ATP synthesis is given by oligomycin-sensitive oxygen consumption (white bracket). The maximal respiratory rate driven by β-hydroxybutyrate and leucine can be estimated by the extent to which these substrates can rescue UK5099-inhibited respiration (green bracket); [glucose], 10 mM; [pyruvate], 1 mM; [β-hydroxybutyrate], 3 mM; [leucine], 2 mM; [UK5099], 100 nM. $n = 5$ technical replicates. A.A., antimycin A; Gluc., glucose; Pyr., pyruvate; Rot., rotenone. (c) Concentration–response curve showing that neurons can maintain mitochondrial ATP synthesis upon MPC inhibition with β-hydroxybutyrate (β-HB) and leucine (Leu.) present in the assay medium. Concentrations as in b. $n = 5$. (d) Schematic showing how isotopically labeled glucose (blue), β-hydroxybutyrate (pink), or leucine (green) can be used to measure incorporation from a given substrate into TCA cycle intermediates via generation of acetyl CoA. AsAT, aspartate aminotransferase; LDH, lactate dehydrogenase; mito., mitochondrial; PDH, pyruvate dehydrogenase. (e) Top, isotopomer spectral analysis (ISA) provides a model for understanding how precursor molecules contribute to a newly synthesized, polymerized product. The schematic depicts how acetyl CoA units from a uniformly labeled glucose tracer contribute to de novo palmitate synthesis. Bottom, mass isotopomer distribution (MID) of palmitate from uniformly labeled glucose after 24 h reveals incorporation of two-carbon units into newly synthesized palmitate. $n = 3$ technical replicates ± SD. (f and g) MPE of labeled carbon into succinate (f) and fumarate (g) shows incorporation of glucose, β-hydroxybutyrate, and leucine into TCA cycle pools. Nc, Neuro-c rich medium; Nc + β-HB, Neuro-c rich medium with 2 mM β-hydroxybutyrate. Data are presented as mean ± SEM and $n = 4$ unless otherwise stated. *, $P < 0.05$.

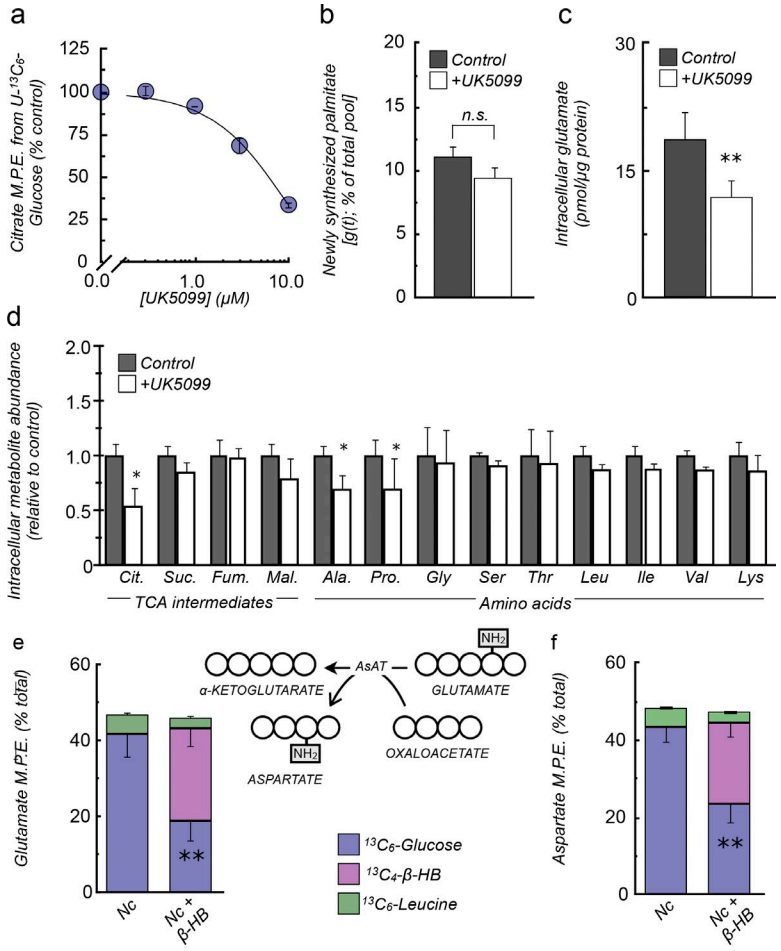

Figure S2. **Inhibition of mitochondrial pyruvate uptake can adjust the abundance and composition of the neuronal glutamate pool while maintaining metabolic rates.** (a) Concentration–response curve of citrate MPE in response to increasing UK5099 concentrations shows that pyruvate carrier inhibition severely restricts glucose incorporation into the TCA cycle. $n = 3$. (b) Newly synthesized palmitate, estimated by isotopomer spectral analysis (ISA), shows that rates of de novo lipogenesis [$g(t)$] are unchanged by UK5099. Values were calculated using uniformly labeled glucose, β-hydroxybutyrate, and leucine as substrates for each preparation of neurons. (c) Quantitative measurements of glutamate abundance confirm that intracellular levels decrease upon 10 µM UK5099 treatment for 24 h. (d) For conditions as in c, there is no broad change in levels of amino acids or TCA cycle intermediates apart from decreases in citrate, alanine, and proline. (e and f) MPE of labeled carbon into glutamate (e) and aspartate (f) shows incorporation of glucose, β-hydroxybutyrate, and leucine into TCA cycle pools. Nc, Neuro-c rich medium; Nc + β-HB, Neuro-c rich medium with 2 mM β-hydroxybutyrate; [UK5099], 10 µM for 24 h. Data are presented as mean ± SEM and $n = 4$ unless otherwise specified. Ala., alanine; Cit., citrate; Fum., fumarate; Mal., malate; Pro., proline; Suc., succinate. *, $P < 0.05$; **, $P < 0.01$; n.s., not significant.

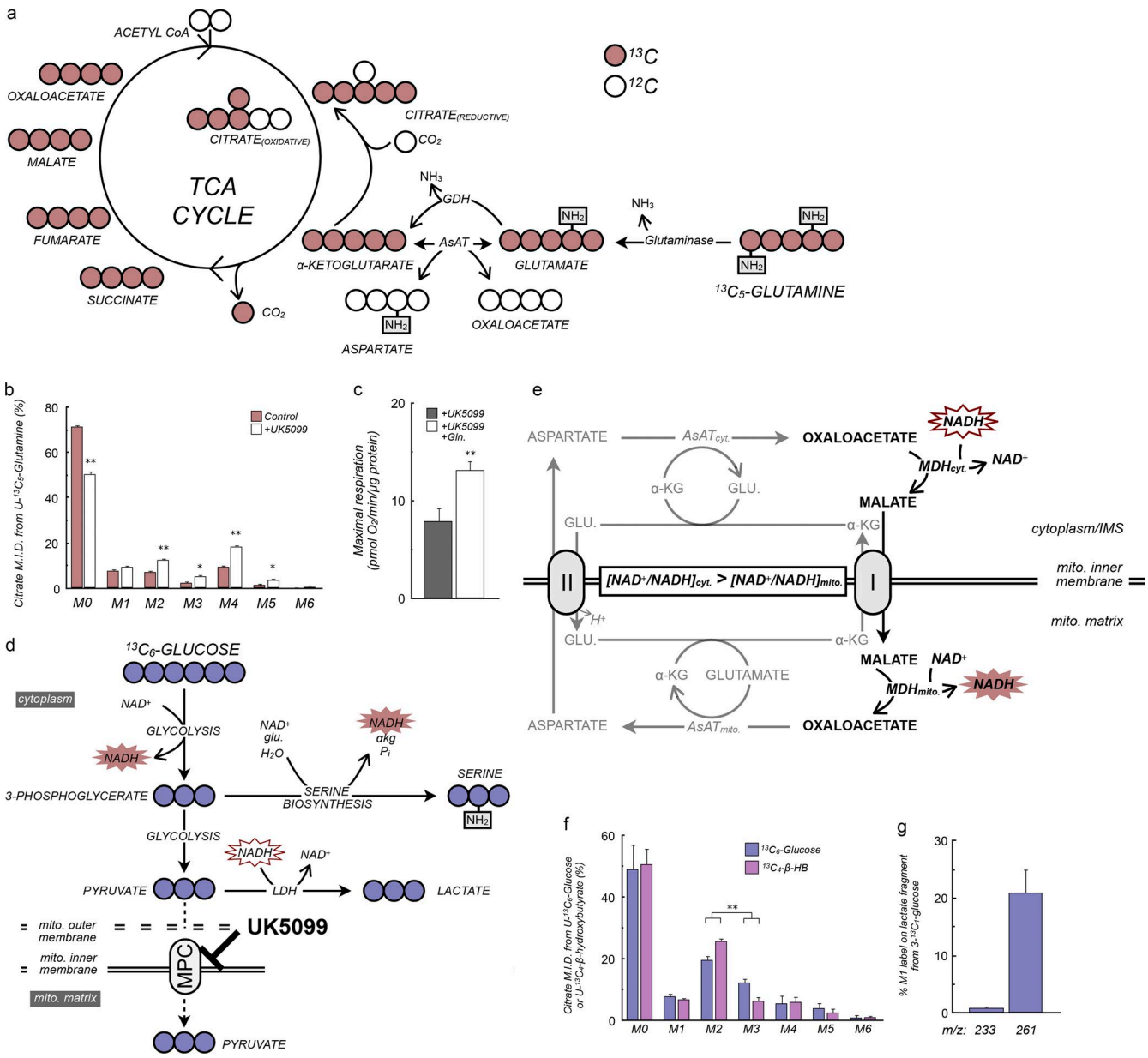

Figure S3. **Glutamine/glutamate oxidation is preferentially increased upon neuronal MPC inhibition.** (a) Schematic showing how [U-$^{13}C_5$]glutamine is incorporated into the TCA cycle by oxidative metabolism as well as reductive carboxylation. GDH, glutamate dehydrogenase; AsAT, aspartate aminotransferase. (b) Mass isotopomer distribution (MID) of citrate from a [U-$^{13}C_5$]glutamine tracer after UK5099 treatment shows that oxidative metabolism of glutamine is increased (M4). Low levels of reductive carboxylation (M5) are increased as well. (c) Maximal, FCCP-stimulated respiration in Neuro-c containing 10 mM glucose, 1 mM pyruvate, and 300 μM UK5099 is increased upon addition of 2 mM glutamine (Gln). 10 μM MK801 is present to prevent excitotoxic injury from spontaneous glutamine deamidation. (d) Schematic showing enrichment from [U-$^{13}C_6$]glucose into serine, pyruvate, and lactate. Cytoplasmic conversion of glucose into pyruvate and serine produces NADH, whereas LDH oxidizes NADH, regenerating NAD^+ and allowing glycolytic turnover. GLU., glutamate; LDH, lactate dehydrogenase; mito., mitochondrial. (e) Schematic showing dependence of the malate-aspartate shuttle on cytoplasmic and mitochondrial redox status. In general, the cytoplasmic pyridine nucleotide pool is more oxidized than the matrix pool. A more reduced cytoplasm could favor the mitochondrial oxidation of glutamate, driving the cytoplasmic malate dehydrogenase toward malate production and lowering the difference in redox status between the cytoplasmic and mitochondrial NAD^+/NADH pools. α-KG, α-ketoglutarate; I, malate-α-ketoglutarate antiporter; II, glutamate-aspartate antiporter; IMS, intermembrane space; MDH, malate dehydrogenase. (f) Citrate MID from a [U-$^{13}C_6$]glucose tracer or a [U-$^{13}C_4$]β-hydroxybutyrate tracer shows that these substrates are incorporated into the TCA cycle at roughly equal levels (1-M0 is broadly similar). Glucose can enter the TCA cycle via acetyl CoA (associated with M2 from a fully labeled tracer) and anaplerotic reactions (associated with M3). Therefore, an increased M3/M2 ratio from glucose relative to β-hydroxybutyrate (which enters only as acetyl CoA) provides a cursory indication of glucose anaplerosis. (g) Use of a [3-$^{13}C_1$]glucose tracer to accurately measure glucose anaplerosis requires labeling to be on the first carbon (C1) of pyruvate. To exclude the possibility that label from this tracer is redistributed to C2 or C3 via the pentose phosphate pathway and subsequently incorporated into the TCA cycle via PDH, we examined enrichment patterns in two lactate fragments: *m/z* 233 (which retains only C2 and C3) and *m/z* 261 (which retains C1, C2, and C3 [Vacanti et al., 2014]). Marginal labeling (<1%) was observed in the 233 fragment, whereas substantial labeling was observed in the 261 fragment. This demonstrates that labeling of TCA cycle intermediates from the [3-$^{13}C_1$]glucose tracer is almost entirely attributable to glucose anaplerosis. Data are presented as mean ± SEM and $n = 4$. *, $P < 0.05$; **, $P < 0.01$. [UK5099], 10 μM for 24 h.

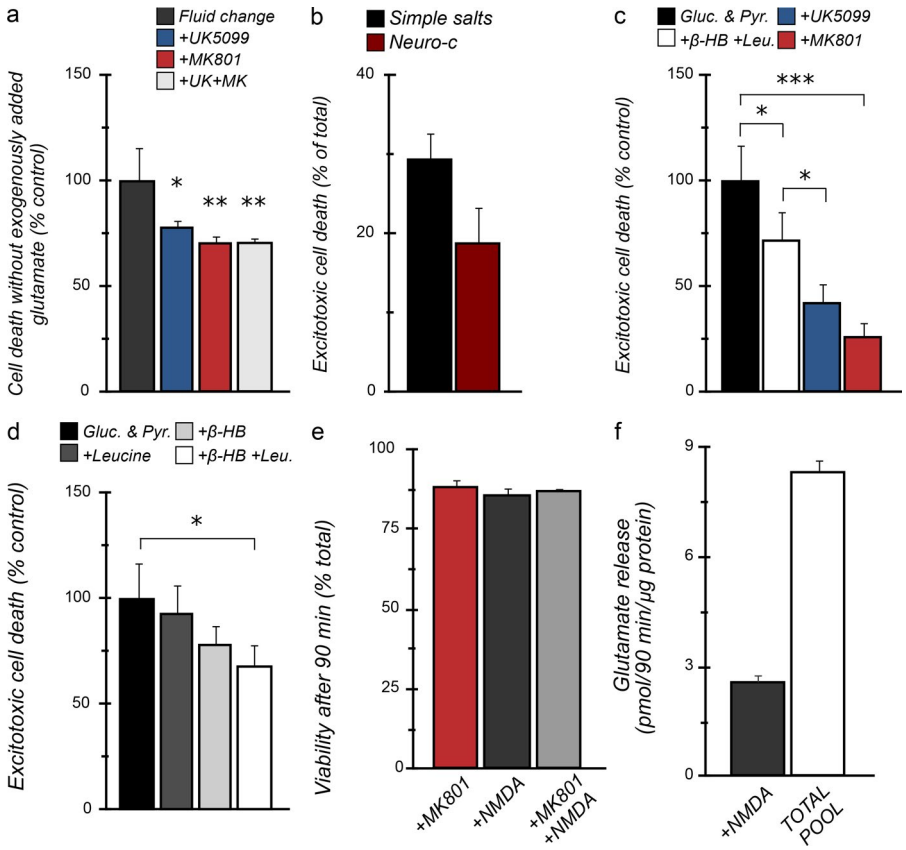

Figure S4. **Adjusting neuronal substrate metabolism can protect from glutamate excitotoxicity.** (a) Excitotoxic injury in vitro can be mediated by the endogenous glutamate pool. Cell death in the absence of exogenously added glutamate during toxicity assays in Neuro-c rich medium qualitatively reproduces the effects of assays conducted with added glutamate (Fig. 6 c): UK5099 is protective and its effects are not additive to protection afforded by MK801. [UK5099], 10 µM; [MK801], 10 µM. (b) Excitotoxicity assays conducted in a simple salts medium cause more excitotoxic cell death, as a percentage of total cells, than assays conducted in Neuro-c rich medium. (c) UK5099 is experimentally neuroprotective in excitotoxicity assays conducted in a simple salts medium: Gluc. & Pyr., 10 mM glucose and 1 mM pyruvate; +β-HB +Leu., 10 mM glucose, 1 mM pyruvate, 2 mM β-hydroxybutyrate, and 2 mM leucine; +UK5099, conditions as in +β-HB +Leu. plus 30 nM UK5099 (medium lacks B27 supplement); +MK801, conditions as in +β-HB +Leu. plus 10 µM MK801. All treatments received 100 µM glutamate as detailed in Materials and methods. (d) Supplementing simple salts medium with nonglucose substrates can be protective from excitotoxic injury. Excitotoxic cell death in simple salts medium is presented with labels as in c where applicable. +β-HB, 10 mM glucose, 1 mM pyruvate, and 2 mM β-hydroxybutyrate; +Leu, 10 mM glucose, 1 mM pyruvate, and 2 mM leucine. All treatments received 100 µM glutamate as detailed in Materials and methods. (e) Neuronal viability is unchanged upon 90-min treatment with 100 µM NDMA. 10 µM MK801 was added 30 min before NMDA addition. $n = 3$. (f) Treatment with 100 µM NDMA for 90 min in Neuro-c evokes release of ~30% of the total releasable glutamate pool. The total releasable pool size was measured by plasma membrane permeabilization with recombinant, mutant PFO ($n = 3$). Data are presented as mean ± SEM and $n = 4$ unless otherwise noted. *, $P < 0.05$; **, $P < 0.01$; ***, $P < 0.001$.

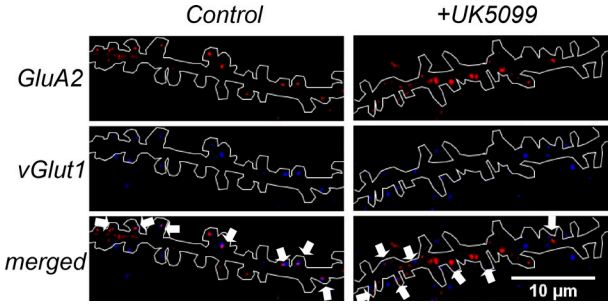

Figure S5. **UK5099 treatment does not compromise synaptic density.** Representative photomicrograph of immunostaining for GluA2 and vGlut1 in dendritic segments. White curves outline the dendritic segments, and white arrows indicate the colocalized puncta of GluA2 and vGlut1.

Reference

Vacanti, N.M., A.S. Divakaruni, C.R. Green, S.J. Parker, R.R. Henry, T.P. Ciaraldi, A.N. Murphy, and C.M. Metallo. 2014. Regulation of substrate utilization by the mitochondrial pyruvate carrier. *Mol. Cell.* 56:425–435. http://dx.doi.org/10.1016/j.molcel.2014.09.024